Redox-Controlled Interconversion between Trigonal Prismatic and Octahedral Geometries in a Monodithiolene Tetracarbonyl Complex of Tungsten

Yong Yan,[†] Perumalreddy Chandrasekaran,[†,‡] Joel T. Mague,[†] Serena DeBeer,[‡,§] Stephen Sproules,*[,§,∥] and James P. Donahue*[,†]

[†]Department of Chemistry, Tulane University, 6400 Freret Street, New Orleans, Louisiana 70118-5698, United States
[‡]Department of Chemistry and Chemical Biology, Baker Laboratory, Cornell University, Ithaca, New York 14853, United States
[§]Max-Planck-Institut für Bioanorganische Chemie, Stiftstrasse 34-36, D-45470 Mülheim an der Ruhr, Germany
[∥]EPSRC National UK EPR Facility and Service, Photon Science Institute, The University of Manchester, Oxford Road, Manchester M13 9PL, U.K.

S *Supporting Information*

ABSTRACT: The tetracarbonyl compounds $[W(mdt)(CO)_4]$ (**1**) and $[W(Me_2pipdt)(CO)_4]$ (**2**) both have dithiolene-type ligands (mdt^{2-} = 1,2-dimethyl-1,2-dithiolate; Me_2pipdt = 1,4-dimethylpiperazine-2,3-dithione) but different geometries, trigonal prismatic (TP) and octahedral, respectively. Structural data suggest an ene-1,2-dithiolate ligand description, hence a divalent tungsten ion, for **1** and a dithioketone ligand, hence W(0) oxidation state, for **2**. Density functional theory (DFT) calculations on **1** show the highest occupied molecular orbital (HOMO) to be a strong W−dithiolene π bonding interaction and the lowest unoccupied molecular orbital (LUMO) its antibonding counterpart. The TP geometry is preferred because symmetry allowed mixing of these orbitals via a configuration interaction (CI) stabilizes this geometry over an octahedron. The TP geometry for **2** is disfavored because W−dithiolene π overlap is attenuated because of a lowering of the sulfur content and a raising of the energy of this ligand π orbital by the conjugated piperazine nitrogen atoms in the Me_2pipdt ligand. A survey of the Cambridge Structural Database identifies other $W(CO)_4$ compounds with pseudo C_{4v} disposition of CO ligands and suggests a d^4 electron count to be a probable common denominator. Reduction of **1** induces a geometry change to octahedral because the singly occupied molecular orbital (SOMO) is at lower energy in this geometry. The cyclic voltammogram of **1** in CH_2Cl_2 reveals a reduction wave at −1.14 V (vs Fc^+/Fc) with an unusual offset between the cathodic and the anodic peaks (ΔE_p) of 0.130 V, which is followed by a second, reversible reduction wave at −1.36 V with ΔE_p = 0.091 V. The larger ΔE_p observed for the first reduction is evidence of the trigonal prism-to-octahedron geometry change attending this process. Tungsten L_1-edge X-ray absorption (XAS) data indicate a higher metal oxidation state in **1** than **2**. Electron paramagnetic resonance data for $[\mathbf{1}]^-$ and $[\mathbf{2}]^-$ are *both* diagnostic of dithiolene ligand-based sulfur radical, indicating that one-electron reduction of **1** *involves two-electron reduction of tungsten and one-electron oxidation of dithiolene ligand.*
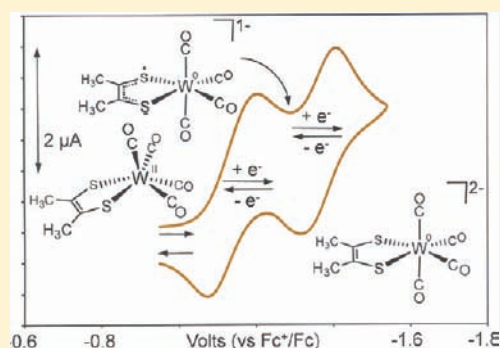
INTRODUCTION

The hexacarbonyls of chromium, molybdenum, and tungsten[1] are classical examples of the octahedral coordination geometry in transition metal complexes. In these complexes, the octahedron is readily understandable as the geometry which optimizes π-backbonding interactions with the CO ligands.[2] The trigonal prismatic (TP) coordination geometry, considerably less common by comparison, is typified by the tris(dithiolene) complexes $[V(S_2C_2R_2)_3]$, (R = H,[3] Ph,[4,5] SCH_2-[6]) $[Mo(S_2C_2R_2)_3]$, (R = H,[7] Me,[8] Et,[9] CF_3[10]), $[W(S_2C_2R_2)_3]$ (R = Me,[11] Ph[12]), and $[Re(S_2C_2Ph_2)_3]$,[13] which have d^1 or d^2 electron counts. Indeed, the first authenticated TP coordination compound was $[Re(S_2C_2Ph_2)_3]$. Recent computational analyses[5,14,15] of these tris(dithiolene)

compounds reveal that the TP geometry is favored over the octahedron by a configuration interaction (CI) which becomes operative between a filled metal-based (d_{z^2}) molecular orbital (MO) and a lower-lying dithiolene ligand π-type MO when one trigonal face of the prism is twisted relative to the other by rotation about the C_3 axis. This twist distortion, commonly known as a Bailar twist (Figure 1),[16] reduces the d_{z^2} and dithiolene ligand π-type MOs to the same symmetry species (a_1 in D_3), which induces their mixing, a destabilization of the occupied d_{z^2}, and a raising of the overall energy of the complex.
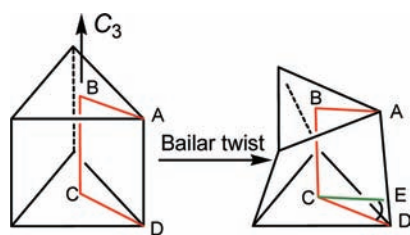
Figure 1. Illustration of the Bailar twist. The Bailar twist angle, Θ, is the torsion angle defined by the line segments AB, BC and CD after rotation of one triangular face of the trigonal prism about the C_3 axis. Segment CE, the projection of BA into the plane of the bottom triangular face, provides an equivalent definition of Θ as the ECD angle.

The distinctly different coordination geometries found for d^6 $[M(CO)_6]$ (M = Cr, Mo, W) and for d^1 and d^2 $[M(S_2C_2R_2)_3]^n$ suggest that the coordination geometries in the heteroleptic compounds $[M(S_2C_2R_2)_2(CO)_2]$ (M = Mo, W) and [W-$(S_2C_2R_2)(CO)_4]$ may be a competition between the preferences of the π-acid ligands and more subtle effects that include d electron count, degree of metal ligand covalency and symmetry of the frontier MOs. These intriguing mixed-ligand species were first prepared by Schrauzer via ligand transfer from $[Ni(S_2C_2R_2)_2]$ to $[M(CO)_6]$ under photolytic conditions.[17] Although Schrauzer illustrated the $[M(S_2C_2R_2)_2(CO)_2]$ (M = Mo, W; R = Me, Ph) compounds as TP species, a formulation shown to be correct in later crystallographic studies of the compounds,[8,11,12] he anticipated the $[W(S_2C_2Me_2)(CO)_4]$ compound to be octahedral.[17,18] However, a recent structural characterization of this compound in our lab revealed that it also is a near-perfect trigonal prism.[11] A preliminary computational analysis of this compound confirmed that the trigonal prism is lower in energy than the octahedral geometry by ~5.1 kcal/mol.[11]

The presence of one dithiolene ligand in $[W(S_2C_2R_2)-(CO)_4]$, a higher formal d electron count, and a lower point group symmetry (C_{2v}) obviously require that the orbital interactions which give rise to the trigonal prism in $[W(mdt)-(CO)_4]$ (1; $mdt^{2-} = S_2C_2Me_2 = $ 1,2-dimethyl-1,2-dithiolate) be rather different than those in d^1 and d^2 tris(dithiolene) complexes $[M(S_2C_2R_2)_3]^n$ complexes. The improved understanding that recent spectroscopic and computational studies have provided[5,14,15] into the electronic structures of the latter set of compounds encourages a deeper analysis of $[W(mdt)-(CO)_4]$ with the expectation that similar insights might be forthcoming. Further motivating this effort are the observations that two species closely related to $[W(mdt)(CO)_4]$, $[W(bdt)-(CO)_4]^{2-}$ ($bdt^{2-} = $ benzene-1,2-dithiolate)[19] and $[Mo-(Me_2pipdt)(CO)_4]$ ($Me_2pipdt = $ 1,4-dimethylpiperazine-2,3-dithione),[20] have crystallographically authenticated *octahedral* geometries. Thus, the overall state of reduction of the compound and the specific nature of the dithiolene-type ligand are important factors in governing the coordination geometry. To better elucidate the electronic structure of $[W(mdt)(CO)_4]$ (**1**), we now augment our initial study with electronic absorption, electron paramagnetic resonance (EPR), and X-ray absorption (XAS) spectroscopic data, further electrochemical data, and a more detailed DFT computational analysis. To assist with comparisons and interpretations, we have also prepared and similarly characterized $[W(Me_2pipdt)-(CO)_4]$ (**2**).

■ EXPERIMENTAL SECTION

Syntheses. Literature procedures were employed for the synthesis of 1,4-dimethylpiperazine-2,3-dithione (Me_2pipdt),[21] [cis-(piperidine)$_2$W(CO)$_4$],[22] and $[Ni(mdt)_2]$.[11] Solvents either were dried with a system of drying columns from the Glass Contour Company (CH$_2$Cl$_2$, *n*-pentane, hexanes) or freshly distilled according to standard procedures[23] (1,2-dichloroethane). Silica columns were run in the open air using 60−230 *μ*m silica (Dynamic Adsorbents).

[W(mdt)(CO)$_4$], 1. The following synthesis is a modification of the original preparation of $[W(mdt)(CO)_4]$ as described by Schrauzer. Under an atmosphere of N$_2$, $[Ni(mdt)_2]$ (0.148 g, 0.5 mmol) and $[W(CO)_6]$ (0.176 g, 0.5 mmol) were combined as solids in a 100 mL Schlenk flask. Dry CH$_2$Cl$_2$ (40 mL) was added to this mixture of solids via syringe. With stirring, the resulting dark purple solution was irradiated for 3 h with a 365 nm wavelength lamp positioned at the side of the flask. The solvent was removed under reduced pressure, and the solid residue was extracted with portions of *n*-pentane (3 × 2 mL). The dark orange extracts were applied directly to the top of a silica gel column packed as a slurry in *n*-pentane and protected from ambient light with a covering of Al foil. Flash elution with *n*-pentane first brought a colorless band of unreacted $[W(CO)_6]$ followed by a dark orange band of **1**, the leading edge of which was yellow. To ensure maximum resolution between **1** and unreacted $[W(CO)_6]$, the colorless eluant immediately preceding the flow of **1** from the column was kept separate. The orange fraction was collected, taken to dryness under reduced pressure, and subjected to vacuum for 24 h to assist removal of traces of unreacted $[W(CO)_6]$. Continued elution of the column as described earlier allowed recovery of a red-violet band of $[W(mdt)_2(CO)_2]$ followed by a green band of $[W(mdt)_3]$. The initial reaction residues left from the *n*-pentane extraction contained an appreciable quantity of $[Ni(mdt)_2]$, which was combined with the unreacted $[W(CO)_6]$ recovered from the chromatography column and subjected to another round of photolysis and workup as just described. Combined yield: 0.052 g of **1** (25% based on $[W(CO)_6]$). Spectroscopic data were identical to those published earlier.[11] Anal. Calcd for C$_8$H$_6$O$_4$S$_2$W: C, 23.20; H, 1.46; S, 15.45%. Found: C, 23.36; H, 1.67; S, 15.34%.

[W(Me$_2$pipdt)(CO)$_4$], 2. A 100 mL Schlenk flask with stir bar was charged with {(CH$_2$N(Me))$_2$C$_2$S$_2$} (0.200 g, 1.147 mmol) and $[W(CO)_4(C_5H_{10}NH)_2]$ (0.534 g, 1.147 mmol) and CH$_2$Cl$_2$ (30 mL) under a N$_2$ atmosphere. The reaction mixture was stirred and progressively changed in color from yellow to blue over a 2 h period. The flask septum was replaced with an oven-dried reflux condenser, and the reaction mixture was heated to 50 °C for 12 h under N$_2$. After being cooled to room temperature, the solvent was removed under reduced pressure. The resulting dark blue solid was washed with 3 × 10 mL of hexanes and dried well under vacuum for 24 h. Crystallization was accomplished by slow diffusion of *n*-pentane vapor into a concentrated 1,2-dichloroethane solution. Yield: 0.437 g, 81%. ^{1}H NMR (ppm in CDCl$_3$): 3.74 (s, 4H, CH_2), 3.50 (s, 6H, *Me*). ^{13}C NMR (CDCl$_3$): 186.38 (s, C≡S), 49.91 (s, CH$_2$), 45.09 (s, CH$_3$). IR (KBr, cm^{-1}): 2001 (vs, CO), 1885 (vs, CO), 1853 (vs, CO), 1832 (vs, CO), 1511 (s), 1400 (m), 1356 (s), 612 (m). Absorption spectrum (CH$_2$Cl$_2$) λ_{max} nm (ε_M): 222 (27800), 278 (16100), 308 (7800), 684 (11000). MS (ESI): 470 (M$^-$). Anal. Calcd for C$_{10}$H$_{10}$N$_2$O$_4$S$_2$W: C, 25.54; H, 2.14; N, 5.95; S, 13.64. Found: C, 23.89; H, 2.21; N, 5.55; S, 12.95.

Physical Methods. Electronic absorption spectra were obtained at ambient temperature with a Hewlett-Packard 8452A diode array spectrophotometer, while IR spectra were taken as pressed KBr pellets with a Thermo Nicolet Nexus 670 FTIR instrument in absorption mode. All NMR spectra were recorded at 25 °C with a Varian Unity Inova spectrometer and referenced to the solvent residual. X-band EPR spectra were obtained using a Bruker ELEXSYS E500 spectrometer whereas S-band and Q-band spectra were recorded on a Bruker ESP 300E spectrometer. The spectra were simulated with the Bruker XSOPHE suite.[24] Electrochemical measurements were obtained with a CHI620C electroanalyzer workstation using a Ag/AgCl reference electrode, a platinum disk working electrode, Pt wire as

auxiliary electrode, and $[^nBu_4N][PF_6]$ as the supporting electrolyte. Under these conditions, the $[Cp_2Fe]^+/Cp_2Fe$ couple consistently occurred at +540 mV. Details regarding collection and processing of X-ray diffraction data and the solution and refinement of the crystal structure of $[W(Me_2pipdt)(CO)_4]$ are deferred to the Supporting Information. Unit cell and refinement data for $[W(Me_2pipdt)(CO)_4]$ are presented in Table 1. X-ray absorption spectra were measured at

Table 1. Crystal Data for 2

formula	$C_{10}H_{10}N_2O_4S_2W$
fw, g/mol	470.17
xtl system	monoclinic
space group	$P2_1/n$
color, habit	blue block
a, Å	10.748(1)
b, Å	10.156(1)
c, Å	25.331(3)
α, deg.	90
β, deg.	92.713(2)
γ, deg.	90
V, Å^3	2762.0(5)
T, K	100
Z	8
R1, wR2^a	0.0186, 0.0388
GoF	1.046

^{a} R1 $= \sum||F_o| - |F_c||/\sum|F_o|$. wR2 $= \{\sum[w(F_o^2 - F_c^2)^2]/\sum[w(F_o^2)^2]\}^{1/2}$; $w = 1/[\sigma^2(F_o^2) + (xP)^2]$, where $P = (F_o^2 + 2F_c^2)/3$.

the Stanford Synchrotron Radiation Lightsource (SSRL) under ring conditions of 3.0 GeV and 60−100 mA. S K-edge data were obtained using the 20-pole wiggler beamline 4-3 and 54-pole wiggler beamline 6-2, and W L-edges on the 20-pole wiggler beamline 7-3, as previously described.[14] Elemental analyses were performed by Midwest Microlab, LLC, of Indianapolis, IN.

Calculations. Geometry optimizations were performed with the Gaussian 09 suite of software[25] and employed the B3LYP functional.[26] The authenticity of each converged structure was confirmed by the absence of imaginary vibrational frequencies. A double-ζ (DZ) basis set with an effective electron core potential (LANL2DZ ECP) was used for tungsten,[27] a triple-ζ basis with two polarization functions was used for sulfur,[28] and 6-311(d,p) basis sets were used for the remaining atoms. Orbital images were created with the use of jmol.[29] The five degree incremental Bailar twist rotations were performed with the use of Chemcraft[30] with intraligand bonds distances held constant for the mdt ligand. Mulliken population analyses were performed with QMForge software package.[31] TD-DFT calculations of the electronic spectra were performed at the B3LYP level of theory with the electronic structure program ORCA.[32] The def2-TVZP[33] basis set was used for all atoms, and a scalar relativistic correction applied using ZORA.[34] The conductor-like screening model (COSMO)[35] was applied to model solvent effects of CH_2Cl_2. Spin density plots were made with the use of Molekel.[36] Time-dependent (TD)-DFT calculation of the sulfur K-pre-edge spectra were performed at the BP86[37] level of theory as previously described[38] using the same atom descriptions used for the electronic spectra. The obtained energies were corrected by an empirical shift of +60.38 eV to match the experimental spectra. Plots were obtained using a 1.0 eV line broadening.

■ RESULTS AND DISCUSSION

Syntheses and Structures. The original preparation of $[W(mdt)(CO)_4]$ (**1**) reported by Schrauzer et al.[17] was a photolysis of $[W(CO)_6]$ in CH_2Cl_2 in the presence of $[Ni(mdt)_2]$, which transfers one of its two dithiolene ligands to tungsten and forms an insoluble, presumably polymeric, metallodithiolene byproduct. Samples of **1** that were isolable

after a chromatography purification were still afflicted with some quantity of unreacted $[W(CO)_6]$. A yield not being clearly indicated, it is inferred to be limited. A recent preparative procedure reported from our group employed $[W(MeCN)_3(CO)_3]$ as starting material (Scheme 1), and while

Scheme 1. Preparation $[W(mdt)(CO)_4]$ (1) and $[W(Me_2pipdt)(CO)_4]$ (2)
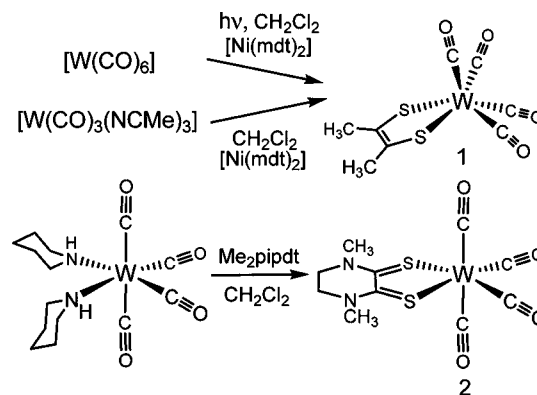
the quantities of **1** obtained were still modest (~15−20%), they were unadulterated with $[W(CO)_6]$. In continuing work with **1**, however, we found that reproducibly higher yields of (~25%) could be obtained from a modification of the original Schrauzer preparation. Differences from the Schrauzer preparation include the use of CH_2Cl_2 as reaction solvent rather than C_6H_6 (Scheme 1), a second iteration of reactivity between $[W(CO)_6]$ and $[Ni(mdt)_2]$ after extraction of a first yield, and recrystallization of **1** from n-pentane such that analytical purity is attained.

Efforts to prepare a monoreduced form of **1** employed 1 equiv of the outer-sphere reagents Cp_2Co or Cp^*_2Co. While immediate reaction leading to a dark red-brown product was observed and presumed to be $[W(mdt)(CO)_4]^-$, this reduced species was not stable enough to permit isolation. This behavior is attributed to both a thermal and light sensitivity that lead to decomposition via ligand dissociation pathways.

The structure of **1**, shown in Figure 2, reveals near-perfect TP coordination geometry, manifested by a Bailar twist angle of 4.0° (Table 2). The narrow range from 2.035(6)−2.043(6) Å that is spanned by the tungsten−carbonyl bond distances emphasizes their chemical equivalence in this arrangement. While the TP geometry now has a considerable degree of precedent among six-coordinate bis(dithiolene) complexes of Mo and W,[8,11,12,39] this configuration has been observed only once before in a six coordinate mono(dithiolene) transition metal complex.[40] This paucity of structurally authenticated examples may be due in part to a general scarcity of mono(dithiolene) ligation in six coordinate complexes, selected examples of which are $[Mo^{IV}O(O=CMe_2)(mnt)(dppe)]$,[41] $[M(OSiPh_3)_2(Me_4phen)(S_2C_2R_2)]$ (M = Mo, R = Ph; M = W, R = Ph, CO_2Me),[42] $[M(CO)_2(PR_3)_2(S_2C_2R'_2)]$ (M = Mo or W),[43] $[PPN]_2[W(bdt)(CO)_4]$ (PPN = bis(triphenyl-phosphineiminium, $Ph_3P=N=PPh_3^+$),[19] and variants of the general type $[\{HB(Me_2pz)_3\}M(X)(S_2C_2R_2)]$ (M = Mo or W, X = PhO^-, SCN$^-$, Et_2NCS^{2-}, O^{2-}, S^{2-}; $S_2C_2R_2$(2-) = arene-1,2-dithiolate or ene-1,2-dithiolate).[44] Each of the foregoing mono(dithiolene) complexes is either octahedral or distorted to some point between octahedral and TP.[43] Prior to the collection of X-ray diffraction data, we had anticipated an
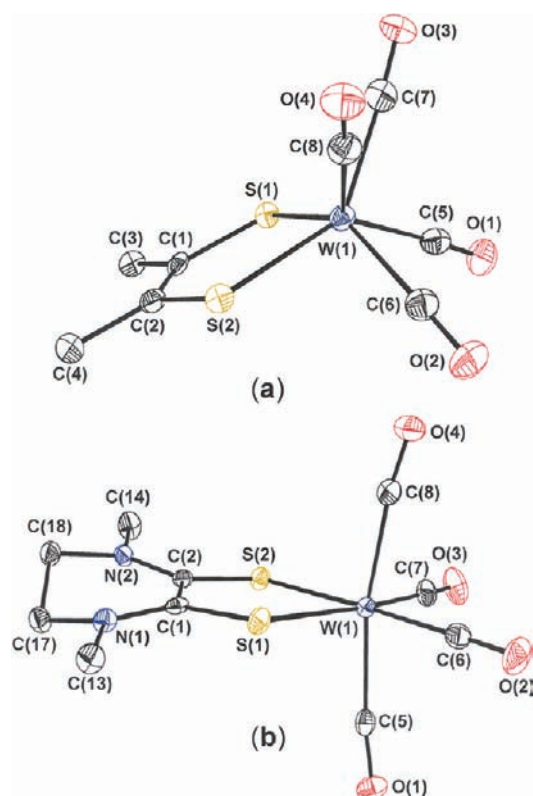
Figure 2. (a) Structure of TP $[W(mdt)(CO)_4]$ (**1**). (b) Structure of octahedral $[W(Me_2pipdt)(CO)_4]$ (**2**). Thermal ellipsoid plots are drawn at the 50% probability level. H atoms are omitted for clarity.

Table 2. Calculated and Experimental (where available) Bond Lengths (Å) and Angles (deg) for $[\mathbf{1}]^{0,1-,2-}$ and $[\mathbf{2}]^{0,1-,2-}$

	$[W(mdt)(CO)_4]$, **1**		$[\mathbf{1}]^-$	$[\mathbf{1}]^{2-}$
	exp.	calc.	calc.	calc.
W−S$_{ave}$	2.361[1]	2.391	2.535	2.623
S−C$_{ave}$	1.744[4]	1.736	1.721	1.773
C−C$_{chelate}$	1.351[8]	1.362	1.383	1.356
W−C$_{ave}$	2.039[3]	2.048	2.023	2.007
W−C$_{orth}$[b]			2.053	2.042
W−C$_{in\text{-}plane}$[c]			1.992	1.972
C≡O$_{ave}$	1.136[4]	1.143	1.159	1.170
C≡O$_{orth}$[b]			1.154	1.162
C≡O$_{in\text{-}plane}$[c]			1.164	1.179
S−W−S	82.38[5]	82.0	80.1	80.7
S−W−C$_{orth}$[b]			92.7	89.3
S−W−C$_{cis}$	86.28[9][d]	86.1[d]	92.7[c]	94.1[c]
S−W−C$_{trans}$	139.77[9][e]	139.4[e]	172.8	174.8
C−W−C$_{cis}$			87.7[f]	90.6[f]
C−W−C$_{cis}$	77.3[1][g]	77.6[g]	94.6[h]	91.2[h]
C−W−C$_{trans}$			173.1	178.3
Θ[i]	4.0	0.0	53.5	55.2
	$[W(Me_2pipdt)(CO)_4]$, **2**		$[\mathbf{2}]^-$	$[\mathbf{2}]^{2-}$
	exp.[a]	calc.	calc.	calc.
W−S	2.5110[4]	2.499	2.565	2.610
S−C	1.687[2]	1.689	1.723	1.778
C−C$_{chelate}$	1.490[3]	1.464	1.416	1.364
W−C$_{orth}$[b]	2.032[2]	2.059	2.048	2.043
W−C$_{in\text{-}plane}$[c]	1.969[2]	2.004	1.982	1.972
C≡O$_{orth}$[b]	1.149[2]	1.147	1.155	1.161
C≡O$_{in\text{-}plane}$[c]	1.156[2]	1.154	1.166	1.178
S−W−S	79.88[1]	79.2	79.4	80.1
S−W−C$_{orth}$[b]	94.43[3]	94.2	91.4	89.9
S−W−C$_{cis}$[c]	94.22[4]	93.0	94.3	94.4
S−W−C$_{trans}$[c]	173.32[4]	172.0	173.7	174.5
C−W−C$_{cis}$[f]	86.20[4]	86.3	88.8	90.1
C−W−C$_{cis}$[h]	91.69[8]	94.9	92.1	91.1
C−W−C$_{trans}$	166.35[8]	169.2	176.5	179.6
Θ[i]	52.8	52.3	53.8	54.8

[a]Experimental bond lengths and angles for **2** are averages from two independent molecules in the asymmetric unit of the unit cell. [b]CO ligands orthogonal to dithiolene ligand plane. [c]CO ligands in dithiolene ligand plane. [d]S−W−C angle for S and C atoms on same trigonal face of trigonal prism. [e]S−W−C angle for S and C atoms on opposite trigonal faces of trigonal prism. [f]Angle between CO ligands, one in and one orthogonal to dithiolene ligand plane. [g]C−W−C angle for CO ligands on same trigonal face of trigonal prism. [h]Angle between CO ligands in dithiolene ligand plane. [i]Bailar twist, defined as rotational angle between trigonal faces of trigonal prism.

octahedral geometry for **1** on the basis that four CO ligands would assert a preference for this configuration because of the presumed optimal π-backbonding interactions with the metal d orbitals enjoyed in this arrangement.

A related tetracarbonyl compound, $[W(Me_2pipdt)(CO)_4]$ (**2**), although not synthesized before, appeared accessible via a procedure analogous to that described for the corresponding molybdenum compound.[20] This compound was selected for synthesis because its properties were expected to provide informative contrast to those of **1**. Preparation of **2** in good yield (~80%) was readily accomplished as anticipated by reaction of dithiooxamide with $[(C_5H_{10}NH)_2W(CO)_4]$ (Scheme 1). Although highly crystalline in form and apparently pure by spectroscopic methods, samples of **2** provided varying elemental analyses outside the generally accepted thresholds for purity. Nevertheless, since its identity is not in question and it has been characterized by a range of other physical methods, compound **2** remains useful for its intended purpose of assisting the interpretation of **1**. An immediate indication that **2** has an electronic structure significantly different from **1**, despite their ostensible similarity of formula, is their pronounced difference in color: blue for the former and yellow-orange for the latter.
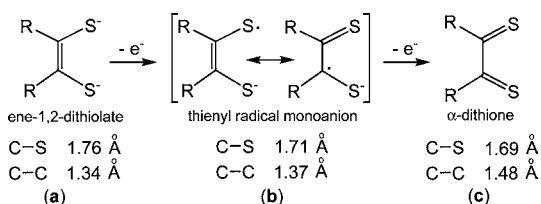
The structure of **2**, shown in Figure 2, is best described as octahedral, as demonstrated by a C−W−C angle that approaches 180° (166.35[8]°, Table 2) and by appreciably different W−C bond distances for the CO ligands *trans* to the Me$_2$pipdt ligand (1.969[2] Å, Table 2) as compared to those orthogonal to the (Me$_2$pipdt)W plane (2.032[2] Å). The S−C (1.687[2] Å) and C−C (1.490[3] Å) bond distances within the coordinated Me$_2$pipdt ligand indicate that the dithione

character of the ligand is largely preserved (Scheme 2). Furthermore, these values are very similar to those reported in a structural characterization of the free ligand,[45] indicating Me$_2$pipdt could be described as a very weak π acceptor. In Scheme 2, bond distances typifying each of the several ligand redox states are presented from structurally characterized nickel bis(dithiolene) complexes with unambiguous dithiolene ligands.[46] The contrast that these S−C and C−C bond distances present to the corresponding values in **1** (1.744[4] Å and 1.351(8) Å, respectively) immediately suggests the essential difference between the two compounds. The structure of **1** reveals a dithiolene ligand that is closer to the reduced ene-

Scheme 2. Redox States of the Dithiolene Ligand, with Approximate C–S and C–C Values Indicated for Each[a]

ene-1,2-dithiolate   thienyl radical monoanion   α-dithione

C–S   1.76 Å   C–S   1.71 Å   C–S   1.69 Å
C–C   1.34 Å   C–C   1.37 Å   C–C   1.48 Å
(a)   (b)   (c)

[a]These bond lengths are taken from the structures of $[Ni(mdt)_2]^n$ (n = 2−, 0 for (**a**) and (**b**), respectively,[46a] and $[Ni(Me_2pipdt)_2]^{2+}$.[46b]

1,2-dithiolate description than otherwise (Scheme 2), while **2** shows the fully oxidized α-dithione variant. Despite being isoelectronic overall, the two compounds have differing tungsten d electron counts arising from differing redox states of their dithiolene-type ligands.

DFT Calculations. The geometry of **1** was optimized in the gas phase beginning with the experimental coordinates. Convergence was obtained for the crystallographic TP C_{2v} symmetric structure with a Bailar twist angle of essentially 0°, a result which indicates that the slightly larger value of 4.0° observed in the crystalline state may be attributable to packing forces. Calculated S–C and C–C$_{chelate}$ bond lengths for the dithiolene ligand agree well with experimental values (Table 2), distances consistent with an ene-1,2-dithiolate formulation of the ligand. Tungsten–sulfur bond lengths are calculated as 0.03 Å longer than those experimentally determined, a difference

that is typical for optimizations with the B3LYP functional.[5,14,47]

Optimization of the structures of the mono- and direduced forms of **1** were also performed despite the unavailability of structural data for these anions. It is noteworthy that the S–C and C–C$_{chelate}$ bond lengths calculated for $[W(mdt)(CO)_4]^-$, $[\mathbf{1}]^-$, are smaller and larger, respectively, than the corresponding values for **1**, implying *oxidation* of dithiolene ligand (cf. Scheme 2) even though *net reduction* has occurred. This computed change is experimentally authenticated by electron paramagnetic resonance (EPR) spectroscopy (vide infra). The dianion exhibits intraligand distances consistent with a coordinated mdt^{2-} ligand highlighting the second reduction as ligand-centered. The lengthening of the W–S bonds from **1** to $[\mathbf{1}]^-$ to $[\mathbf{1}]^{2-}$ reflects decreased π donation from the dithiolene ligand because the metal acceptor orbitals are now filled, $(t_{2g})^6$. Furthermore, interligand repulsion between the highest occupied dithiolene π orbital and those on the CO ligands are also contributing factors. The monoanionic and dianionic species are therefore defined as $[W^0(mdt^{\bullet-})(CO)_4]^-$ and $[W^0(mdt^{2-})(CO)_4]^{2-}$, respectively. Another important outcome of these optimizations is a predicted change of geometry to an octahedron upon reduction. The chief difference between the mono- and dianionic forms of **1** is that interligand angles for the latter more closely approach idealized 90° and 180° values (Table 2). This difference is an expected one, as the ideal octahedron maximizes the backbonding of the π-acidic CO ligands with the tungsten d orbitals in this more electron rich species. Concomitantly, the radical
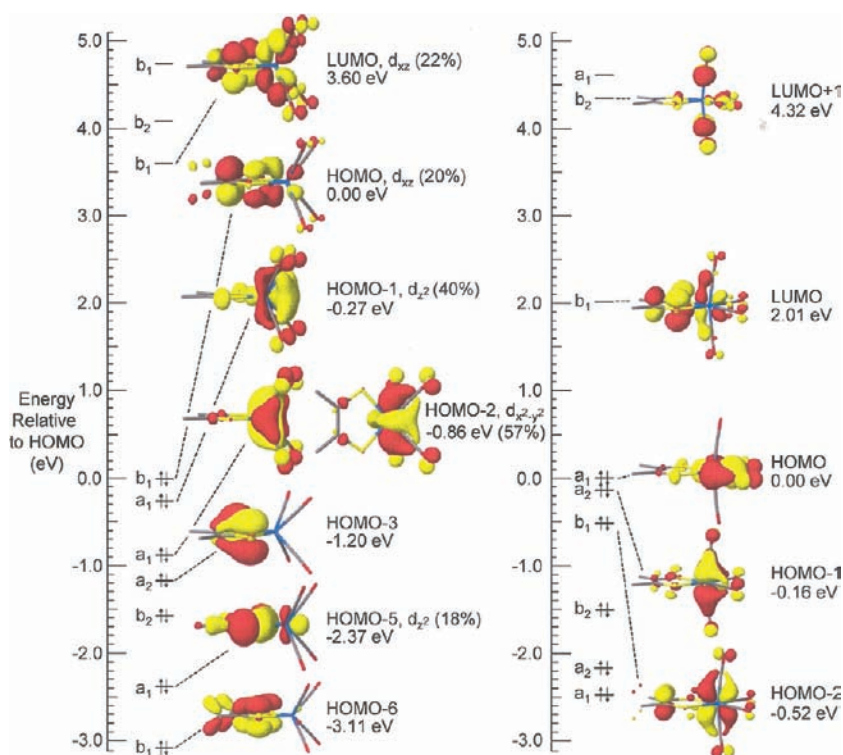

Figure 3. Frontier MOs for TP (C_{2v}) $[W(mdt)(CO)_4]$ (left) and octahedral (C_{2v}) $[W(mdt)(CO)_4]$ right. The C_2 symmetry axis of TP $[W(mdt)(CO)_4]$ is defined as its z axis. The d orbital composition of several MOs is indicated as a percentage. The d_{yz} and d_{xy} orbitals of tungsten contribute to multiple filled and empty MOs (not shown). For clarity, the HOMO-2 for the TP geometry is shown in orthogonal orientations. Orbital energies are relative to the HOMO for each geometry. Contour images are drawn at the 0.05 level. Strong configuration interaction between HOMO and LUMO (both b_1) produces a stabilization of the TP geometry.
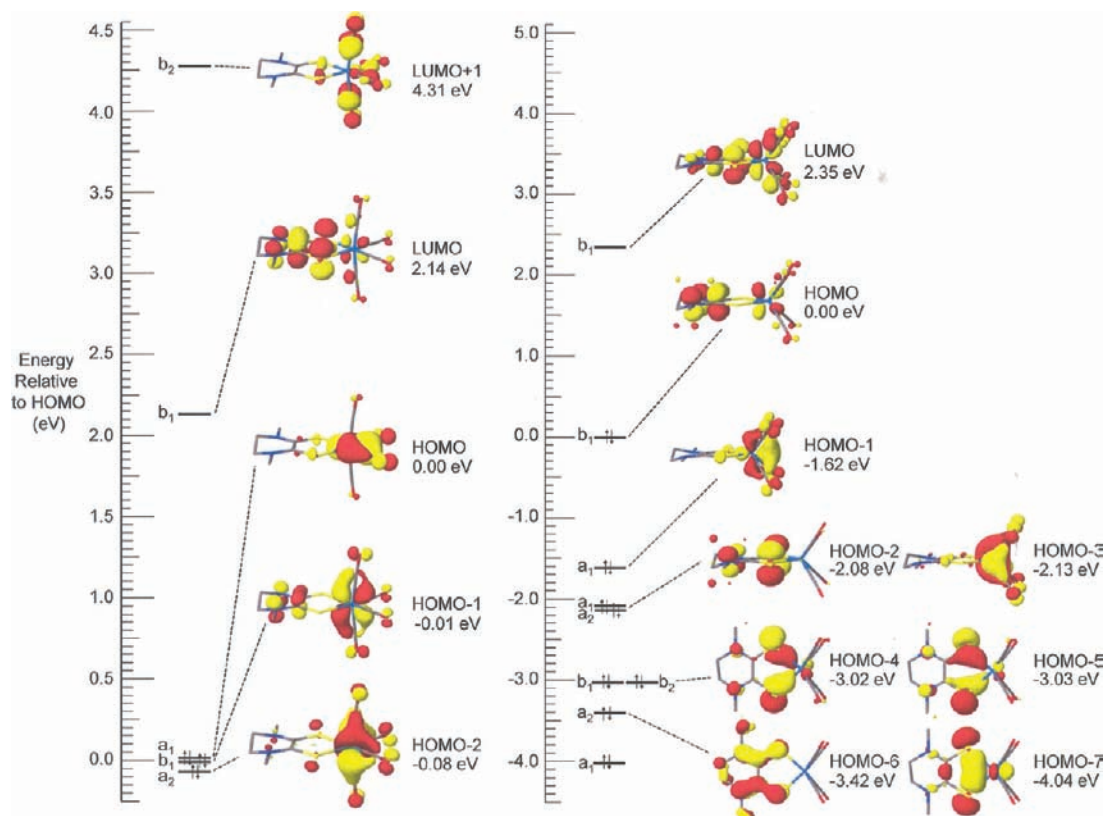
Figure 4. Frontier MOs for octahedral (C_2) [W(Me$_2$pipdt)(CO)$_4$] (left) and TP (C_2) [W(Me$_2$pipdt)(CO)$_4$] right. Orbital energies are relative to the HOMO for each geometry. Contour images are drawn at the 0.05 level. To facilitate comparisons to compound **1**, Mulliken symmetry labels are shown for idealized C_{2v} point group symmetry.

monoanion mdt$^{•-}$ is a significantly weaker π donor than mdt^{2-} and therein no longer stabilizes a W(II) ion.

The [**2**]$^{0,1-,2-}$ series was also geometry optimized, an octahedral configuration being the lowest energy geometry across the series. Calculated interatomic distances for **2** agree well with those determined crystallographically. As the set is traversed from neutral molecule to dianion, the most important set of changes is a closer disposition of the ligands to ideal 90° and 180° interligand bond angles. The *trans* OC−W−CO angle, for example, opens from 169.2° to 176.5° to 179.6° in moving from **2** to [**2**]$^-$ to [**2**]$^{2-}$ (Table 2). This trend is coupled with an increase in the W−S bond lengths (2.499 Å to 2.610 Å) as the compound is successively one-electron reduced. The lengthening of short C−S distances and contraction of the C−C$_{chelate}$ bond length as **2** is reduced confirm the reduction events as ligand-centered such that the reduced forms are formulated as [W^0(Me$_2$pipdt$^{•-}$)(CO)$_4$]$^-$ and [W^0(Me$_2$pipdt^{2-})(CO)$_4$]$^{2-}$, respectively. For [**2**]$^-$, this electronic structure is confirmed spectroscopically.

With the optimized structure of **1** constrained to C_{2v} symmetry, a single point calculation of its electronic structure shows the HOMO to be principally a W−dithiolene π bonding interaction, while the LUMO is its antibonding counterpart but with some admixture of metal → CO backbonding (Figure 3, left). An inspection of these orbitals' symmetry (Figure 3) immediately identifies a basis for the TP coordination geometry. Both HOMO and LUMO have b$_1$ symmetry, which necessitates a configuration interaction (CI) that stabilizes the occupied HOMO and destabilizes the unoccupied LUMO — a second-order Jahn−Teller distortion.[48] The LUMO+2 also belongs to the b$_1$ symmetry species and is

likely contributing to the stabilization of the HOMO with a similar CI, although its magnitude is necessarily smaller because of the greater difference in energy between these orbitals. The upshot of this configuration interaction is a rather significant HOMO−LUMO energy gap of 3.6 eV, an energy difference that is much larger than that between any other adjacent pair of frontier MOs in this molecule. A d electron count for TP **1** is not immediately obvious from Figure 3 owing to the mixed composition of the occupied frontier MOs. As the images in Figure 3 make qualitatively apparent, the HOMO, HOMO-1, HOMO-2, and HOMO-5 all have significant contributions from the tungsten d orbitals. A Mulliken population analysis of these frontier orbitals, summarized in Supporting Information, Table S1, indicates that collectively they account for ~1.6 d orbitals and suggests that a d^4 electron count, limited meaning though it may have in such a highly covalent system, is more pertinent than any alternative count. This conclusion is consistent with the reduced ene-1,2-dithiolate description and W(II) central ion which emerge from the structural data and the XAS data (vide infra).

The foregoing explanation is supported by a single point calculation upon *octahedral* **1**, a calculation performed by replacing the Me$_2$pipdt ligand in optimized **2** with the mdt ligand and slightly adjusting W−S, S−C, and C−C$_{chelate}$ bond distances to produce the lowest energy for this geometry. When constrained to this configuration, the HOMOs are essentially a pair of near-degenerate orbitals from the W t$_{2g}$ set (explicitly a$_1$ and a$_2$ in C_{2v} symmetry).[49] What was the HOMO in TP **1**, corresponds to the HOMO-2 in the octahedral configuration, essentially the W d$_{xz}$ orbital. This orbital is stabilized ~0.5 eV relative to the other t$_{2g}$ orbitals by a subtle metal → dithiolene

π backbonding interaction. The LUMO is again the ligand π^* orbital with b_1 symmetry (Figure 3, right). The considerable W d/CO p character for the HOMOs (60−90%, Supporting Information, Table S2) with considerable π back-donation to the CO ligands, renders the metal best viewed as a W(0) d^6 central atom. The corollary immediately following this conclusion is that oxidation of mdt^{2-} to mdt^0 has occurred to account for the changed d^4-to-d^6 electron count at tungsten. Most importantly, this conformation is 5.3 kcal mol^{-1} more unfavorable than the TP geometry, indicating that the CI lowers the total energy of the molecule. This result is starkly contrasted by calculations of TP and octahedral **2**, where the opposite effect is observed (Figure 4, right). Thus, the perfect trigonal prism for **1** arises from orbital interactions that are maximized in C_{2v} point group symmetry and diminished by any Bailar twist away from $\Theta = 0°$. This description of the nature of the changes which occur is further confirmed by the observation that the frontier MOs for **2** (Figure 4, left), which is experimentally shown to have a fully oxidized dithiolene ligand, are highly similar to those of octahedral **1** (Figure 3, right). Thus, an internal redox exchange between dithiolene ligand and tungsten is governed by geometry interconversion (Scheme 3).

Scheme 3. Internal Redox Change Governed by Interconversion between TP and Octahedral Geometries
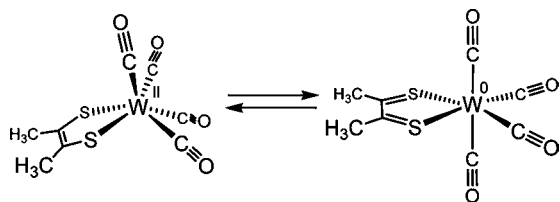
Chemical reduction of TP **1** places an electron into a LUMO that is greatly destabilized in this geometry. Thus, the energetic stabilization that is the basis for a trigonal prism is removed, and the octahedral geometry becomes overall lower in energy. The basis for the geometry change is rendered more clear by a Walsh-type diagram in which the energies of the frontier molecular orbitals for **1** are plotted as a function of incremental Bailar twist angles that move the trigonal prism to an octahedral geometry (Figure 5, top). The principal changes occurring as this geometry change is effected are a raising of the energy of the HOMO, HOMO-1, and HOMO-2 collective set, clearly the largest contribution to the energy difference stabilizing the trigonal prism vis-à-vis the octahedron in **1**, and an even greater lowering of the energy of the W−dithiolene π^* LUMO. The energy crossovers that bring the HOMO in TP **1** to the HOMO-2 in octahedral **1** are seen to occur in the $\Theta = 25-40°$ region. A plot of total energy versus Θ (Figure 5, bottom) shows a smooth ascent in energy to $\Theta = 60°$ and an absence of any maximum that would suggest the participation of competing effects as noted for $[Mo(bdt)_3]^{0,1-}$.[15]

Although Figures 3 and 5 and the discussion attending them offer explanation for the greater stability enjoyed by the TP geometry over the octahedral geometry in **1**, the high degree of likeness between the MOs for octahedral **1** (Figure 3, right) and octahedral **2** (Figure 4, left) present the question as to why the trigonal prism is not similarly stabilized for **2**. Some insight into the question is found by grafting the reduced Me$_2$pipdt^{2-} ligand, taken from $[\mathbf{2}]^{2-}$, onto the W(CO)$_4$ fragment from

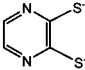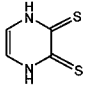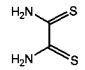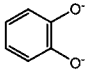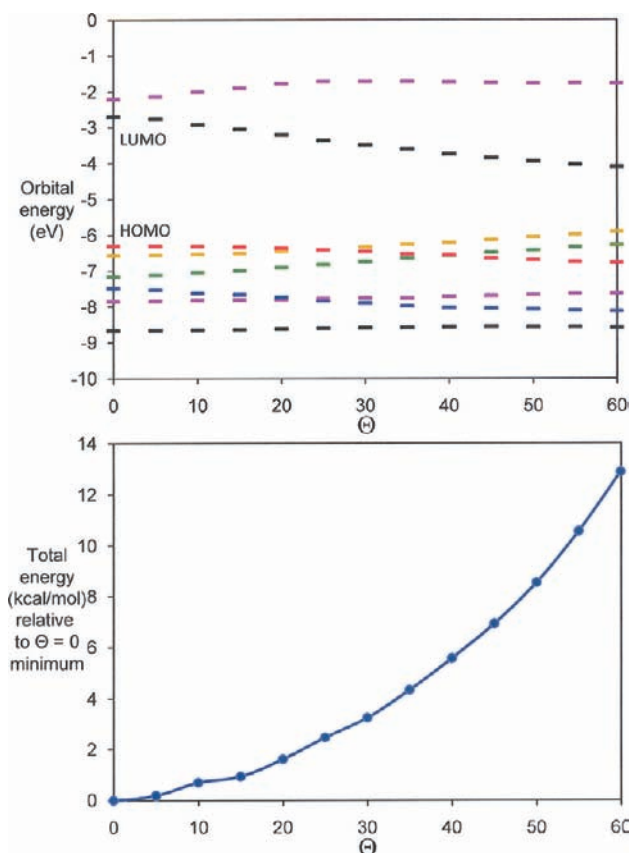**Figure 5.** Walsh diagram illustrating energies of the frontier MOs (top), and total energy (bottom) of **1** as function of Bailar twist angle, Θ. The total energy at $\Theta = 60°$ differs from the ~5.3 kcal/mol greater energy for octahedral **1** over TP **1** noted in Table 3 because the Bailar twist operation itself does not carry all interligand C−W−C and S−W−C angles to values corresponding to an energy minimum for a given value of Θ.

optimized TP **1** (with W−S bond lengths of 2.391 Å as computed for **1**) and executing a single point calculation of the electron structure for TP **2**. An energy level diagram accompanied by illustration of key frontier MOs is given in Figure 4, right. While some of the MOs for TP **2** closely resemble their counterparts in TP **1**, for example, the LUMO, HOMO-1, and HOMO-2, a key difference between the two compounds in this geometry lies with the composition of the HOMO. In contrast to the HOMO for TP **1** (Figure 3, left), that for TP **2** (Figure 4, right) completely lacks any sulfur p character. The consequences of this absence of sulfur p character are complete disengagement of metal-dithiolene π backbonding, a diminution of covalency between tungsten and dithiolene ligand, an increase in tungsten d orbital character to the relative composition of the HOMO, and an overall destabilization of this orbital. The conjugated piperazine ring reduces the sulfur content of this ligand π^* orbital, and therefore the back-donation is greatly attenuated because of decreased W−S overlap. The magnitude of this destabilization can be gauged by noting that for both TP **1** and **2**, the LUMO and HOMO-1 are highly similar in appearance and nature, have a near identical energy difference of ~3.9 eV, and offer a frame of reference for the difference in energy of these two HOMOs. If the HOMO-1 is taken as a zero point, it is seen that the HOMO in TP **2** is destabilized by ~1.3 eV relative to the HOMO in TP **1**. It is noteworthy that, despite the absence of

Table 3. Computational Results for $[WL(CO)_4]^n$ Compounds

| $[WL(CO)_4]^n$ | | Opt. geom | Point grp. | Calc. bond lengths, Å | | Orbital symmetry | | b_1–b_1 (b-b) gap, eV^a | $\Delta,^b$ |
L	n			C–X (X = S, O, N)	C–C chelate	HOMO	LUMO		kcal mol^{-1}
mdt^c	0	TP	C_{2v}	1.736	1.362	b_1	b_1	3.60	5.3
mdt	1-	Oct	C_{2v}	1.721	1.383	b_1	b_2	4.85	29
mdt	2-	Oct	C_{2v}	1.773	1.356	b_1	b_2	4.13	65
bdt^d	0	TP	C_{2v}	1.752	1.404	$b_1{}^e$	b_1	3.69	11
mnt^f	0	TP	C_{2v}	1.740	1.370	b_1	b_1	3.81	9.7
pdt^g	0	TP	$C_2{}^h$	1.744	1.369	b	b	3.29	6.5
[pyrazine-2,3-dithiolate structure]	0	TP	C_{2v}	1.749	1.411	$b_1{}^e$	b_1	3.69	14
[dihydropyrazine-dithione structure]	0	Oct	C_{2v}	1.675	1.450	b_1	b_1	1.84	23
Me$_2$pipdt^i	0	Oct	$C_2{}^j$	1.689	1.464	a,b,a^k	b	2.15	17
Me$_2$pipdt	1-	Oct	$C_2{}^j$	1.723	1.416	b	A	3.51	29
Me$_2$pipdt	2-	Oct	$C_2{}^j$	1.778	1.364	b	A	2.97	78
[dithiooxamide structure]	0	Oct	$C_2{}^j$	1.681	1.434	a,b^l	B	2.22	11
[catecholate structure]	0	TP	C_{2v}	1.347	1.405	b_1	b_1	3.23	4.2
bipy	0	Oct	C_{2v}	1.360	1.471	a_1	b_1	2.59	36

^{a}Difference in energy between the highest occupied and lowest unoccupied orbitals of b_1 (or b) symmetry. ^{b}Difference by which optimized geometry is computed to be lower in energy than the TP or Oct alternative. ^{c}mdt^{2-} = 1,2-dimethyl-1,2-dithiolate. ^{d}bdt^{2-} = benzene-1,2-dithiolate. ^{e}The b_1 label corresponds to the HOMO-1, which is nearly degenerate with the HOMO. ^{f}mnt^{2-} = maleonitriledithiolate. ^{g}pdt^{2-} = 1,2-diphenyl-1,2-dithiolate. ^{h}C_{2v} symmetry is disrupted by the angles of the Ph substituents with respect to the WS$_2$C$_2$ chelate ring. ^{i}Me$_2$pipdt = 1,4-dimethyl-piperazine-2,3-dithione. ^{j}C_{2v} symmetry is disrupted by pyramidalization at the nitrogen atoms. ^{k}The HOMO are the near-degenerate t_{2g} set of orbitals. ^{l}The HOMOs are two near-degenerate orbitals of the t_{2g} type.

sulfur p character to the HOMO for TP **2**, it still has the same symmetry as the LUMO (both b_1 in pseudo C_{2v} symmetry). Thus, these orbitals are also subject to a CI as in TP **1**, but this is insufficient to offset other destabilizing influences on the HOMO as noted above.

The preceding discussion regarding orbital interactions fully complements the crystallographic data indicating differing dithiolene ligand redox states as the key difference between TP **1** and octahedral **2**. The governance of coordination geometry may be viewed as a question of ligand reducibility, versus reducibility of the W(CO)$_4$ fragment, which in turn hinges upon the ligand π^* orbitals being available at the right energy to draw electron density away from tungsten and create a favorable π bonding interaction. Since the TP geometry found for **1** does not appear to arise from any special attribute of the ligand beyond the relative ease with which it is reduced, the suggestion emerges that this coordination geometry should not be unique to **1** but should instead be generally preferred in $[WL(CO)_4]$ where L is comparable to mdt in its ability to

oxidize W(CO)$_4$ via appropriate orbital interactions. It follows that the octahedron should be the preferred geometry in $[WL(CO)_4]$ compounds when oxidized L is more stable than d^4 W(CO)$_4$. These suppositions have been canvassed in a computational survey of real or plausible charge neutral $[WL(CO)_4]$ compounds, the results of which are organized in Table 3. The critical indicators in this table are the computed C–X (X = S, O, or N) and C–C$_{chelate}$ bond lengths. The TP geometry is found for all the mono(dithiolene) tetracarbonyl complexes that optimize with reduced ene-1,2-dithiolate ligands (S–C $\approx$ 1.74 Å, C–C$_{chelate}$ $\approx$ 1.37 Å), while all complexes bearing dithiooxamide type ((R$_2$N)C=S)$_2$ ligands (S–C $\approx$ 1.69 Å, C–C$_{chelate}$ $\approx$ 1.46 Å) adopt the octahedral configuration. It is noteworthy that $[W(O_2C_6H_4)(CO)_4]$ optimizes to a TP geometry and a catecholate type ligand (O–C $\approx$ 1.35 Å. C–C $\approx$ 1.41 Å),[50] rather than an o-semiquinone ligand (O–C $\approx$ 1.31 Å, C–C $\approx$ 1.44 Å).[51] The L$^{(2-)}$W$^{(2+)}$ formalism implied by this result reinforces the idea that a d^4 electron count at tungsten is requisite for the TP

configuration in these compounds. Furthermore, examination of the frontier MOs for optimized $[W(O_2C_6H_4)(CO)_4]$ reveals a HOMO and LUMO with essentially the same nature as the corresponding orbitals for TP **1**. An octahedral geometry is computed and observed[52] for $[W(bpy)(CO)_4]$ because the 2,2′-bipyridyl ligand, although reducible, is not nearly as readily reduced as the $W(CO)_4$ fragment.[53]

Another perspective on the relationship between metal d electron count and coordination geometry is given by a survey of crystallographically characterized $W(CO)_4$ compounds that occur in the Cambridge Structural Database. Our analysis includes dimetallic compounds and multimetal clusters without restriction on coordination number at tungsten in the $W(CO)_4$ moiety. Excluding penta- and hexacarbonyl tungsten compounds, and correcting for redundant database entries, molecules with the minimal $W(CO)_4$ fragment number 537 occurrences.[54] The great majority of these compounds (457) are six-coordinate compounds in which the two remaining coordination sites have a cis disposition. For convenience, this structure type is defined here as fac-$W(CO)_4$ or cis-$W(CO)_4$ (Figure 6). It follows from the arrangement of ligands that one

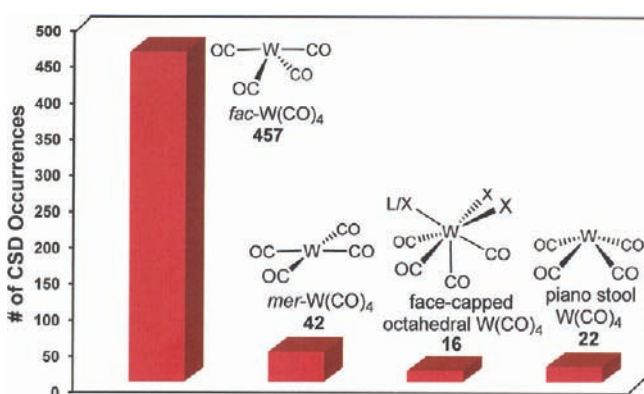**Figure 6.** Distribution of $W(CO)_4$ compounds in the Cambridge Structural Database. This analysis excludes $W(CO)_6$ and $W(CO)_5$ compounds, which number 1437 hits, and is adjusted for redundant occurrences of the same compound with same unit cell.

C−W−C angle is ~180° and the remaining five are near 90°. Another set of $W(CO)_4$ compounds, designated mer-$W(CO)_4$, has a completely planar arrangement of the $W(CO)_4$ group. It is clear that both metal−ligand bonding interactions and steric considerations have some role in governing the choice of this structure type. A W(0) formal oxidation state (d^6 electron count) is a feature shared by the fac-$W(CO)_4$ and mer-$W(CO)_4$ compounds. A smaller set of $W(CO)_4$ compounds (16) are seven-coordinate face-capped octahedral W(II) species in which a triangular face defined by three CO ligands is capped by the fourth CO. In most of these cases, the opposing trigonal face of the octahedron is occupied by three halide ligands such that the complex is monoanionic and C_{3v} symmetric overall.

A fourth and final category of $W(CO)_4$ complexes is composed of compounds with a pseudo C_{4v}-symmetric piano stool fragment similar to **1**, where OC−W−CO angles are ~77 and 125° (Figure 6). In these instances, except for **1**, either three additional ligands or some relatively bulky or planar species, such as a cyclobutadienyl dianionic ligand, complete the coordination sphere around tungsten.[55,56] As the only member of this set that is six-coordinate, **1** is the only compound that would be described as TP. Notwithstanding

their ostensible dissimilarities with varying coordination numbers, it is clear that d^4 W(II) appropriately describes tungsten in most, if not all, members of this group. Since this electronic description is the apparent common denominator in this set of $W(CO)_4$ compounds, it is probable that it is indeed a d^4 electron count that promotes the pseudo C_{4v}-symmetric $W(CO)_4$ piano stool configuration.

In this context, it is worth notice that two electron oxidation of $[W(CO)_6]$ by SbF_5 in HF-SbF_5 produces a TP $[W(CO)_6]^{2+}$ core structure that is capped on one rectangular face by a weakly coordinating SbF_6^- anion.[57] This observation, in conjunction with the foregoing survey of structural data on $W(CO)_4$ compounds and the computational studies of others,[56] bolsters the idea that the metal d electron count plays a critical role in governing the choice of trigonal prism vs octahedron in six-coordinate $W(CO)_4$ compounds. Although TP geometry is common among bis- and tris(dithiolene) complexes of the transition metals, our results do not decisively indicate that the trigonal prism in **1** arises from a particular feature unique to the mdt^{2-} ligand beyond its capacity to stabilize a d^4 W(II) ion by a strong π interaction.

Electrochemistry. The cyclic voltammogram of **1** reveals only irreversible features when scanned in the reducing direction with MeCN as solvent. When CH_2Cl_2 is used for the voltammetry, markedly better behavior is observed (Figure
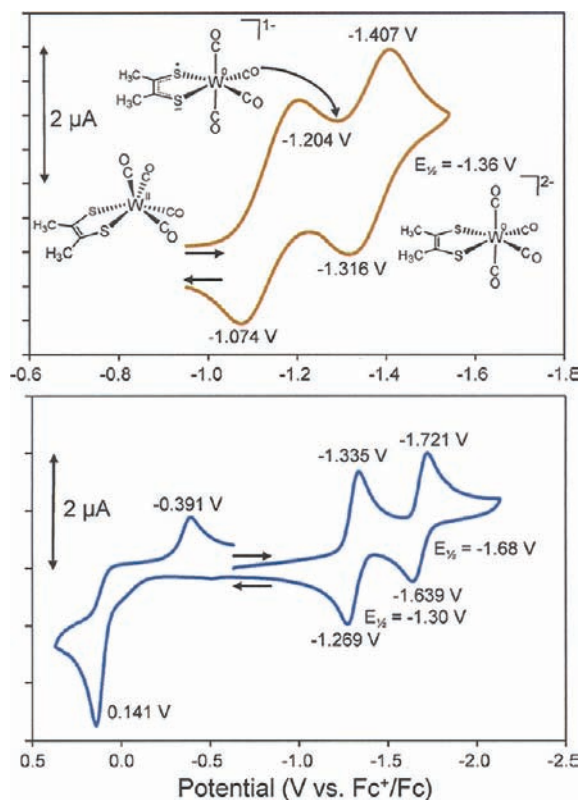

Figure 7. Cyclic voltammograms of **1** (top) and **2** (bottom) in CH_2Cl_2 with $[^nBu_4N][PF_6]$ supporting electrolyte at 100 mV/s. The CV for **2** was run at −25 °C.

7) which we attribute to improved stability against loss of CO in this weakly coordinating solvent. An initial cathodic wave with maximum at −1.20 V is closely followed by a second reduction wave with peak maximum at −1.41 V. On the return side of the scan, corresponding anodic peaks are observed at

−1.32 V and −1.07 V. The peak-to-peak separation for the second reduction wave is 0.091 V, a ΔE_p value that is typical of reversible processes under these experimental conditions. However, the anodic return wave for the first reduction process is offset from the cathodic maximum by a noticeably greater value of 0.130 V (Figure 7, top panel).

This situation of a *second* reduction process that is *more reversible* in appearance than an *initial*, apparently *quasireversible*, reduction is unusual but is consistent with a facile trigonal prism to octahedron geometry change. If a rapid structural change to an octahedral geometry occurs upon one-electron reduction of **1**, then a noncorrespondence of the potential for maximum current upon reoxidation (E_a) relative to the cathodic maximum would be expected. As the forgoing computations have indicated (Figures 3 and 5), and as intuition would suggest on the basis of π-backbonding considerations, the octahedron better stabilizes $[\mathbf{1}]^-$ than does the trigonal prism. Thus, the $[\mathbf{1}]^- \rightarrow [\mathbf{1}]^0 + e^-$ reoxidation requires a potential ∼40 mV *more oxidizing* (−1.07 V rather than −1.11 V) than it would if no structural change were operative. No atypical changes in $E_{1/2}$ values or in the appearance of the voltammogram are observed at scans rates up to 1.0 V/s, indicating that this geometry change is rapid on the time scale of the voltammetry experiment.

The cyclic voltammogram of **2** reveals two successive one-electron reductions (Figure 7, bottom panel) but at potentials moderately more reducing (−1.30 V, −1.68 V) than required for **1**. Reversible-appearing behavior for the second reduction wave was only observable at low temperature (−25 °C). The peak-to-peak separations observed in these two waves (ΔE_p = 0.066 V, 0.082 V) contrast with the corresponding values for **1** (ΔE_p = 0.130 V, 0.091 V) and indicate an absence of structural change as predicted by the geometry optimizations for $[\mathbf{2}]^{0,1-,2-}$ (Table 2). Compound **2** also displays a 2-electron oxidation process, presumably metal-centered, which is quasi-reversible by controlled potential electrolysis but irreversible in appearance in the cyclic voltammogram (Figure 7, bottom panel).

Electronic Spectroscopy. The most immediate and arresting difference between **1** and **2** is the striking contrast in colors: gold-yellow for the former but dark blue for the latter. The electronic absorption spectra for the two compounds are overlaid in Figure 8. The lowest energy absorptions of the two compounds, which are chiefly responsible for their perceived colors, have comparable molar extinction coefficients of ∼15,000 M^{-1} cm^{-1} but markedly different energies. In CH_2Cl_2 as solvent, the lowest energy excitation for **1** occurs at 408 nm while that for **2** is observed at 669 nm.

Deconvolution of the experimental electronic absorption spectrum for **1** (Supporting Information, Figure S1, top) fits one broad peak at the observed maximum. A time-dependent (TD) DFT calculated spectrum for **1** discloses the lowest energy excitation to be a symmetry allowed b_1 (HOMO) → b_1 (LUMO) transition (Supporting Information, Figure S1, bottom), albeit slightly blue-shifted with a maximum at 380 nm (29,390 cm^{-1}). The calculated intensity closely matches the experimental intensity of this transition. The very mixed nature of the MOs involved does not permit a simple description of the nature of the transition. This excitation has both metal-to-ligand charge transfer (MLCT) and intraligand charge transfer (ILCT) character, as the HOMO and LUMO are both comprised of a mixture of W d_{xz} and mdt π^* orbitals. The
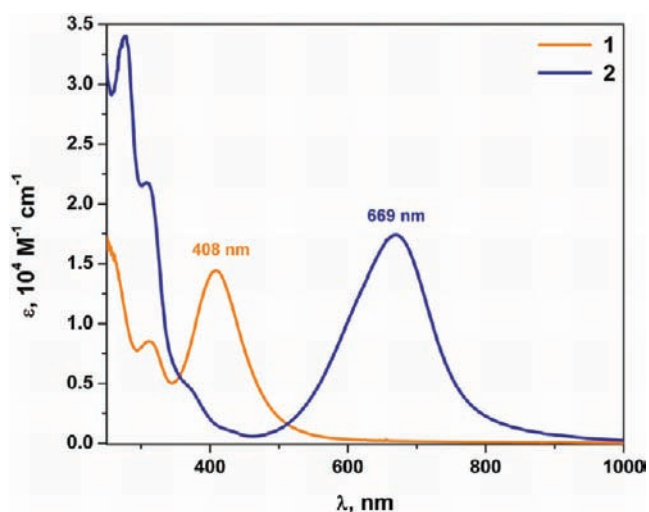

Figure 8. Electronic absorption spectra of **1** (orange) and **2** (blue) recorded in CH_2Cl_2 solutions at ambient temperature.

composition of the LUMO carries a significant admixture of CO π^* character as well (Figure 3, left).

A similar deconvolution of the experimental absorption spectrum for **2** identifies two distinct transitions contributing to the asymmetric absorption profile at 669 nm (Supporting Information, Figure S2, top). TD-DFT calculations (Supporting Information, Figure S2, bottom) only yielded one transition contributing to this peak, again slightly blue-shifted to 619 nm (16,160 cm^{-1}). Similar to **1**, and as identified in a study of closely related $[Mo(Me_2pipdt)(CO)_4]$,[20] this excitation is the symmetry allowed $b_1 \rightarrow b_1$ MLCT transition from the filled d_{xz} orbital to the empty Me_2pipdt π^* LUMO. In these calculations, the d_{xz} is the HOMO, though gas-phase calculations position it as HOMO-2 (Figure 4, left), highlighting the near-degeneracy of the t_{2g} set whose ordering is affected by minor geometric distortions supplied by the dielectric continuum. This point is apparent by the previously noted solvent dependence of the MLCT band that correlates inversely with solvent polarity (Supporting Information, Figure S3, Table S3). This negative solvatochromism is typical of zerovalent $[ML(CO)_4]$ compounds (M = Cr, Mo, W; L = bpy, phen) and is attributed to an excited state with an electric dipole moment that is appreciably diminished relative to that of the ground state.[58,59]

The energy of the MLCT band in these $WL(CO)_4$ complexes is a direct measure of the HOMO−LUMO gap and therein the energy of the ligand π^* orbital. For instance, dark blue **2** with an absorption maximum at 669 nm has the lowest π^* orbital, and therefore would serve as better π acceptor ligand than related bidentate N,N′-donor ligands: $^iPr_2$-ATI (diisopropylaminotropionate, λ_{max} = 580 nm, violet),[60] biq (biquinoline, λ_{max} = 573 nm, violet),[61] pyca (pyridine carbaldehyde, λ_{max} = 524−573 nm, red-violet),[62] bpy (2,2′-bipyridine, λ_{max} = 450−574 nm, red-brown)[58,63] and phen (1,10-phenanthroline, λ_{max} = 486 nm, red-orange).[64] Saturated bidentate ligands such as dithiophosphonate and tetramethylethylenediamine (tmeda) are pale yellow since they lack a π^* acceptor orbital for a MLCT transition.[65] The gold-yellow color of **1** is a direct indication that the equivalent π^* orbital in mdt is filled and that the ligand is in its dianionic form. If an octahedral geometry were present, the dithiolene ligand would be fully oxidized, mdt^0, and the calculated electronic spectrum positions the MLCT band at 510 nm (Supporting Information,

Figure S4). With such an electronic configuration the compound would be deep red. Therefore, the electronic and molecular structure of any $W(CO)_4$-based compound can be readily assessed by its color.

Although reduced forms of **1** and **2** were not amenable to isolation, the monoanions of both could be generated coulometrically and spectroscopically observed (Figure 9).
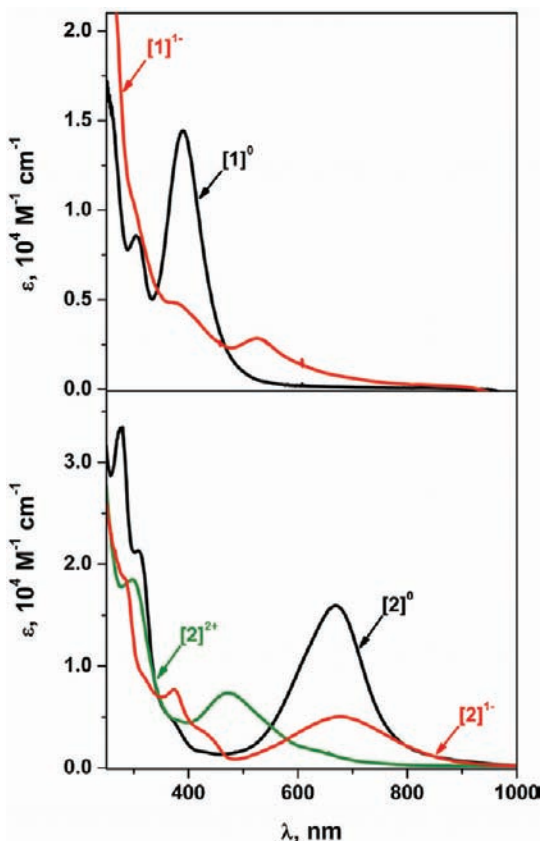

Figure 9. Electronic spectra of electrochemically generated [W(mdt)-$(CO)_4]^{0/1-}$ (**1**) species (top) and $[W(Me_2pipdt)(CO)_4]^{2+/0/1-}$ (**2**) species (bottom) in CH_2Cl_2 (0.10 M [$^nBu_4N$][PF_6]) at −25 °C.

Formation of [**1**]$^-$ from **1** is marked by disappearance of the maxima at 316 and 408 nm and the onset of a lower intensity peak at ~540 nm and an unresolved shoulder at ~400 nm (Figure 9, top). When generated in situ from **2**, [**2**]$^-$ is observed to have an absorption maximum slightly lower in energy than the 669 nm absorption in **2** with a molar extinction coefficient approximately one-third its magnitude (Figure 9, bottom; Supporting Information, Figure S5). Coulometric generation of [**2**]$^{2+}$ is marked by disappearance of the absorption maximum at 669 nm and appearance of a new maximum at 472 nm (Figure 9, bottom), but the transition between spectra is not attended by a stable isosbestic point (Supporting Information, Figure S6). Coulometric re-reduction of [**2**]$^{2+}$ to **2** restores the 669 nm absorption band but with a prominent shoulder at ~800 nm, indicating that chemical decomposition of [**2**]$^{2+}$ is operative on the time scale of this experiment (Supporting Information, Figure S7).

Sulfur K-edge XAS. The pre-edge features in sulfur K-edge X-ray absorption spectra arise from excitations of electrons from the sulfur 1s orbital to acceptor MOs bearing some degree of sulfur 3p character. One of the valuable insights offered by

the method is quantitative assessment of metal–ligand covalency and diagnosis of sulfur-based radicals. Transitions gain intensity according to the degree of sulfur p orbital content in the acceptor orbital. Figure 10 presents experimental sulfur
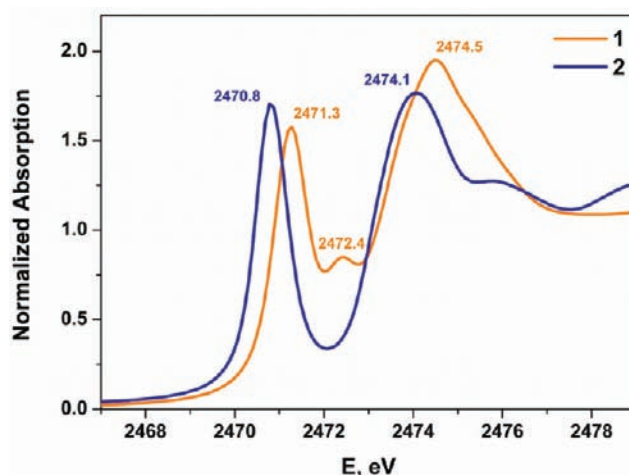

Figure 10. Normalized S K-edge spectra for **1** and **2**.

K-edge spectra for **1** and **2**. These spectra show intense pre-edge features of similar intensity at 2471.3 and 2470.8 eV for **1** and **2**, respectively. However, owing to the differences between **1** and **2** in effective nuclear charge of both W and S atoms, Z_W^{eff} and Z_S^{eff}, and coordination geometry (and hence ligand field), the two spectra do not contrast simply. The lower Z_W^{eff} (W^0) and higher Z_S^{eff} (thione sulfur) for **2** would contribute to a higher energy transition in the pre-edge region than for **1**, which has a higher Z_W^{eff} (W^{II}) and lower Z_S^{eff} (thiolate S).[66] However, the pre-edge energy for **2** is 0.5 eV lower in energy than that for **1**, and this ordering is therefore attributed to ligand field effects which supersede the influence of Z_W^{eff} and Z_S^{eff}.

Sulfur K-pre-edge spectra calculated by TD-DFT for **1** and **2**, after a +60.38 eV empirical correction, reproduce exactly the first pre-edge transition seen experimentally and indicate that the acceptor orbital in both cases is the LUMO (Figure 11). The HOMO−LUMO configuration interaction in **1** substantially elevates the energy of its LUMO (vide supra), and clearly is the primary reason for the 0.5 eV higher pre-edge transition energy for **1**. The LUMOs for both **1** and **2** have substantial contribution from the organic π system of the dithiolene ligand, although that for **1** has significant composition from the tungsten d_{xz} orbital and the CO ligands and is qualitatively a rather different orbital than the LUMO for **2** (cf. Supporting Information, Tables S1−S2). The experimental spectrum for **1** shows an additional feature at 2472.4 eV, which may be a S 1s → C−S π^* seen previously in the [$Ni(mdt)_2$]$^{0/1-/2-}$ series.[67] Higher energy absorption maxima in the sulfur K-edge spectra for **1** and **2** are observed at 2474.1 and 2474.5 eV, respectively (Figure 10). Multiple excitations comprise the absorbance in the 2472.5−2474.5 eV region, but their specific identity is less reliably given than the lowest energy transition.

Tungsten L-edge XAS. Figure 12 displays the tungsten L_1-edge X-ray absorption spectra for **1** and **2**, which involve excitations from the metal 2s orbitals. Although these spectra do not show pre-edge features because of poor edge resolution due to a short core-hole lifetime, their rising edge energies (involving W_{2s} → W_{6p} transitions or excitations to the
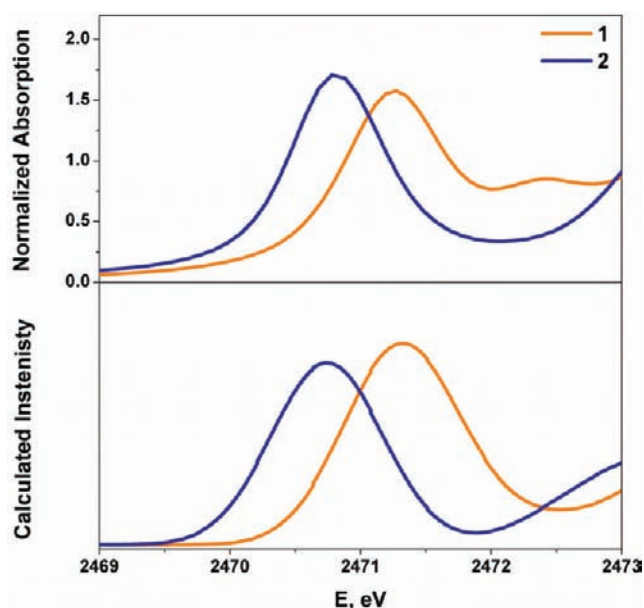
Figure 11. Experimental (top) and calculated (bottom) S K-pre-edge XAS spectra of **1** and **2** obtained from BP86 TD-DFT calculations. Calculated intensity in arbitrary units.
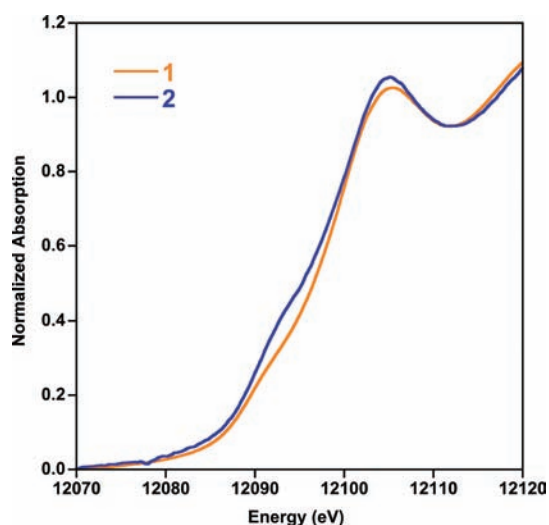

Figure 12. Tungsten L_1-edge spectra of **1** and **2**.

continuum) are more sensitive to Z_W^{eff} than those in the tungsten $L_{2,3}$-edge spectra. The higher rising edge energy of ~1.5 eV observed for **1** vs **2** is qualitatively consistent with the higher metal oxidation state (lower d electron count) suggested by the crystallographic data and computational results. The tungsten L_2-edge and L_3-edge X-ray absorption spectra (Supporting Information, Figure S8) involve transitions from tungsten 2p orbitals to MOs with tungsten 5d character. These transitions are subject to more complicated effects, such as multiplet effects, which do not allow for straightforward analysis.

EPR Spectroscopy. The one-electron reduced forms of **1** and **2** are paramagnetic ($S = {}^1/_2$), and therefore EPR spectroscopy provides a useful means of both corroborating the DFT data and contrasting the inherent electronic structure of these very different dithiolene ligands. The X-band EPR spectrum of $[1]^-$ recorded at 30 K is shown in Figure 13. This
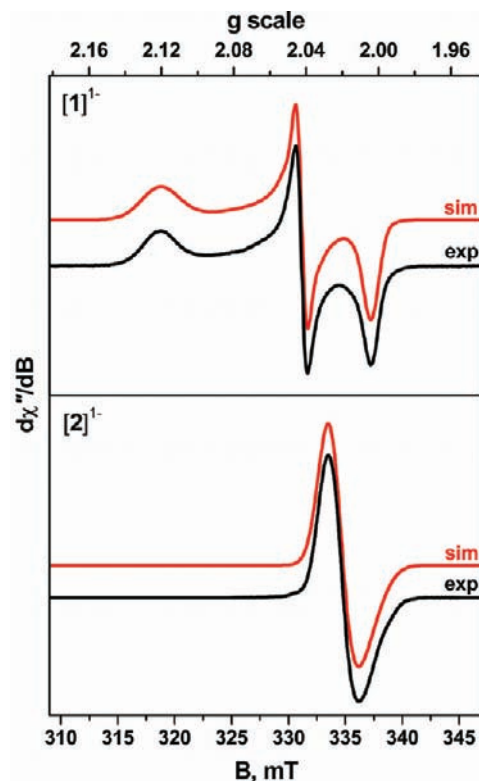

Figure 13. X-band EPR spectra of electrochemically generated $[1]^-$ (top) and $[2]^-$ (bottom) recorded in CH_2Cl_2 at 30 K. The simulation is shown in red with the experimental data in black (experimental conditions, $[1]^-$: frequency, 9.4361 GHz; power, 0.63 mW; modulation, 0.4 mT. $[2]^-$: frequency, 9.4269 GHz; power, 0.063 mW; modulation, 1.0 mT).

rhombic spectrum is characterized by $g = (2.1154, 2.0360, 1.9991)$ with overall anisotropy, $\Delta g = 0.116$. Shoulder features that are faintly visible on g_2 and g_3 are attributed to the magnetic hyperfine interaction of the ^{183}W ($I = {}^1/_2$, 14.31% natural abundance) isotope, $A = (0, 24, 30) \times 10^{-4}$ cm^{-1}. There was no evidence for hyperfine centered on g_1 even at S-band frequencies. The inclusion of g- and A-strain parameters in the simulation improved the overall line shape.

The frozen solution X-band spectrum of $[2]^-$ could not be more different from that of **1** (Figure 13, bottom) with nearly isotropic g-values ($g = 2.0165, 2.1032, 1.9992$). These parameters were obtained from a multifrequency approach (S-, X-, Q-band); the spectra and simulations are depicted in Supporting Information, Figure S9. Overall, the anisotropy ($\Delta g = 0.017$) is substantially smaller than for $[1]^-$, and a true axial spectrum is only evident at Q-band (Supporting Information, Figure S9, bottom). The hyperfine interaction was left out of the spin-Hamiltonian because the low anisotropy and intrinsic line width obscure any such features at all three bands. However, fluid solution measurements on chilled (200 K) samples at S- and X-band (Supporting Information, Figure S10 and S11) revealed a multitude of hyperfine lines for $[2]^-$. These observations are very similar in appearance to results of an elegant EPR spectral study by Deplano, Robertson, and co-workers of the free ligand radical and its Ni(II) complex.[68] A second derivative spectrum at S-band was distinguished by a heptet of pentets that could only arise from coupling of six protons ($I = {}^1/_2$, 99.99% natural abundance) and the two ^{14}N ($I = 1$, 99.64% natural abundance) nuclei of the Me$_2$pipdt$^{\bullet-}$

ligand. Simulation of this pattern yielded isotropic hyperfine values of $A_H = 4.4 \times 10^{-4}$ cm^{-1} and $A_N = 0.7 \times 10^{-4}$ cm^{-1}, respectively (Figure 14). The additional splittings in the spectra
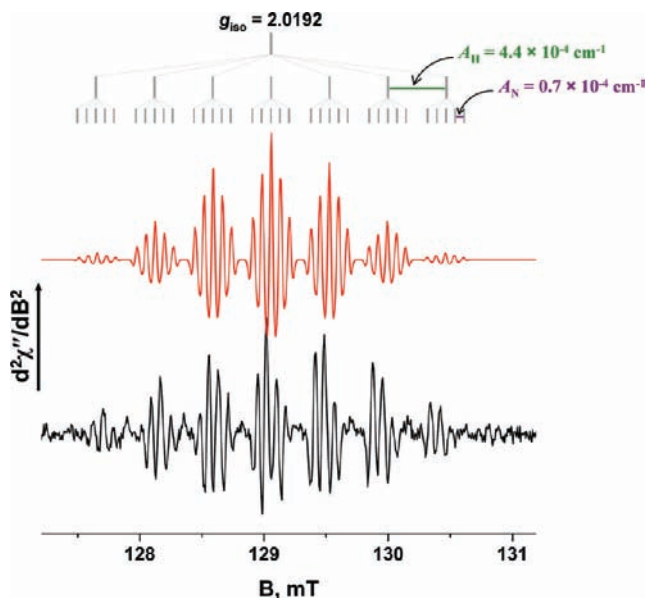

Figure 14. Second derivative S-band spectrum of $[\mathbf{2}]^-$ recorded in CH$_2$Cl$_2$ at 200 K (conditions: frequency, 3.6464 GHz; power, 20.1 mW; modulation, 0.04 mT). Experimental spectrum is shown in black, and the simulation depicted in red. The hyperfine splitting generating the heptet of pentets is described above.

are presumably due to the four methylene protons of Me$_2$pipdt$^{\bullet-}$, though we have not attempted to simulate these highly complex multiline spectra.

The EPR parameters obtained for $[\mathbf{1}]^-$ and $[\mathbf{2}]^-$ demonstrate the inherent difference between these two dithiolene ligands. Despite the same overall electronic structure, $[W^0(\text{dithiolene}^{\bullet-})(CO)_4]^-$, the different hyperfine splitting for each reveals that the unpaired electron in $[W^0(\text{mdt}^{\bullet-})(CO)_4]^-$ resides mainly on the sulfur atoms of mdt$^{\bullet-}$ in a π^* orbital with 19% d$_{xz}$ character that drives the g-anisotropy. In contrast, the conjugated nitrogen atoms of the piperazine ring in $[W^0(\text{Me}_2\text{pipdt}^{\bullet-})(CO)_4]^-$ relocate electron density away from the metal and leads to coupling with the nitrogen atoms and methyl group protons. The experimental spin density at the protons can be estimated by $\rho_H = A_{iso}/1419$ MHz to give a value of 0.0092.[69] The spin density distributions shown in Figure 15 corroborate the spectral parameters with negligible spin density on the W atom in $[\mathbf{2}]^-$, whereas substantial spin density is discharged on to the W atom in $[\mathbf{1}]^-$ from the coordinated sulfur atoms of mdt$^{\bullet-}$. The average spin distribution on the methyl protons of 0.0036 is in reasonable agreement with the experiment, and furthermore, the calculated spin density of the methylene protons of 0.0021 would give rise to a coupling ($\sim 1 \times 10^{-4}$ cm^{-1}) too small to be unambiguously verified in this system.

Although the spin in $[\mathbf{1}]^-$ has a modest presence on the tungsten atom and the CO ligands, and although the unpaired spin in $[\mathbf{2}]^-$ experiences coupling to the ^{1}H and ^{14}N nuclei of the Me$_2$pipdt ligand, the radicals in these two monoanions have a common nature in being largely based on the dithiolene-type ligand. The spin density plots in Figure 15 emphasize their essential similarity. Thus, the consequence of *reducing* **1**, in
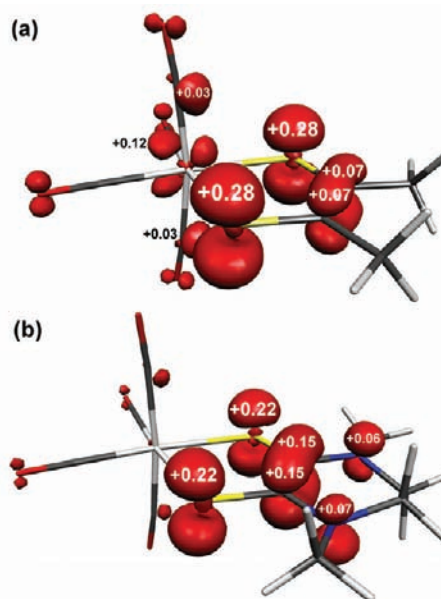

Figure 15. Spin density plots of (a) $[\mathbf{1}]^-$, and (b) $[\mathbf{2}]^-$ from spin unrestricted DFT calculations together with values from the Mulliken analyses.

which the dithiolene ligand is largely reduced, is that the dithiolene ligand becomes *oxidized* during the trigonal prism-to-octahedron transformation and the attending internal redox chemistry between metal and ligand. Such nuanced redox chemistry is one of the more interesting, subtle, and potentially useful aspects of systems with noninnocent ligands. We are aware of only two prior instances[15,70] of analogous behavior, both involving reordering of closely spaced frontier molecular orbitals rather than geometry changes, but the number of documented instances is likely to grow.

■ CONCLUSION

In summary, we find that C_{2v} TP **1** enjoys this unanticipated coordination geometry principally by producing a favorable d^4 electron count at tungsten (II) via the formation of a symmetry allowed W−dithiolene π interaction. Superimposed over this d electron count is a stabilizing CI, which is engaged in the TP geometry but not in the octahedral alternative. Although its effect is stabilizing, this CI appears not to be the dominant factor. We note, for example, that **2** is not TP, even though HOMO and LUMO would both commute with b$_1$ symmetry in this geometry. Although it is still important, the role of CI appears to be secondary to the issue of the reducibility of the noncarbonyl ligand (L) vis-à-vis tungsten in $[WL(CO)_4]$ compounds via a positioning of the ligand π^* system such that effective oxidation of metal can occur. The key role of d electron count at tungsten is demonstrated by the observation of coordination geometry change from trigonal prism to octahedron when **1** is reduced. This ostensibly simple one-electron reduction of the complex in actuality induces a *two-electron reduction at tungsten and an offsetting one-electron oxidation of dithiolene ligand*, even though the ligand is best described as fully reduced at the start. The correctness of this description is affirmed not only computationally but also by experimental data, notably EPR spectra of $[\mathbf{1}]^-$ indicating the presence of dithiolene radical monoanion (Scheme 2).

A recent detailed study of trigonally prismatic complexes identifies this geometry as constituting $\sim$1% of structurally

authenticated 6-coordinated complexes.[71] Within this set, few examples occur which have multiple (>2) π-acid ligands, the only examples being $[Ta(C\equiv C-Si^tBu)_6]^-$,[72] and d^4 **1**, the subject of the present study. A principal reason for this rarity is that complexes with multiple π-acid ligands have high d electron counts that disfavor the trigonal prism. This study was restricted to six-coordinate complexes. Our survey of $W(CO)_4$ compounds, broadened to include all coordination numbers, identifies a modest but noteworthy number of compounds which share with **1** a pseudo C_{4v} symmetric piano stool $W(CO)_4$ fragment and, we assert, a common d^4 electron count at tungsten.

It is generally true that the dithiolene ligand supports redox-active metal complexes. Compound **1** is no exception to this generality even though one-electron reduction of the complex occasions a rather nonobvious electronic reorganization. The facile, reversible, redox-controlled geometry change observed for the $[\mathbf{1}]^{0/1-}$ couple, as illustrated in Figure 7, offers the conceptual basis for molecule-scale switching or gating. Molecule-scale devices which involve redox-controlled rotation of a ring about an axis or translational movement of a ring along the length of a molecular string through which it is threaded have been described.[73] Similarly, metallocarborane complexes in which two carborane ligands change their relative disposition by rotation as a function of redox state have been advanced as a basis for rotary molecular motors.[74] Our observations of the redox-controlled geometry change in **1** create the possibility that suitably modified variants, for example, with bidentate isonitrile ligands substituting CO ligands for enhanced stability, could be simpler and more accessible alternatives to these other systems.

ASSOCIATED CONTENT

Ⓢ Supporting Information

Full description of crystal growing procedures, data collection and processing, and structure solution and refinement. Complete crystallographic data for **2** in CIF format. Gaussian deconvoluted experimental and calculated electronic absorption spectra. Electronic absorption spectra from coulometric measurements of **2**. Tungsten $L_{2,3}$-edge XAS spectra for **1** and **2**. Multifrequency EPR spectra for $[\mathbf{2}]^{1-}$. Supplementary figures as noted in text. Results of Cambridge Structural Database Survey organized by structural type of the $W(CO)_4$ fragment. This material is available free of charge via the Internet at http://pubs.acs.org.

AUTHOR INFORMATION

Corresponding Author

*E-mail: sproules@mpi-muelheim.mpg.de (S.S.), donahue@tulane.edu (J.P.D.).

ACKNOWLEDGMENTS

REFERENCES

(1) (a) Rees, B.; Mitschler, A. *J. Am. Chem. Soc.* **1976**, *98*, 7918−7924. (b) Mak, T. C. W. *Z. Krystallogr.* **1984**, *166*, 277−281. (c) Heinemann, F.; Schmidt, H.; Peters, K.; Thiery, D. *Z. Krystallogr.* **1992**, *198*, 123−124.

(2) Cotton, F. A.; Wilkinson, G. In *Advanced Inorganic Chemistry*, 5th ed.; Wiley & Sons: New York, 1988; pp 58−62.

(3) Kondo, M.; Minakoshi, S.; Iwata, K.; Shimizu, T.; Matsuzaka, H.; Kamigata, N.; Kitagawa, S. *Chem. Lett.* **1996**, 489−490.

(4) (a) Eisenberg, R.; Gray, H. B. *Inorg. Chem.* **1967**, *6*, 1844−1849. (b) Eisenberg, R.; Stiefel, E. I.; Rosenberg, R. C.; Gray, H. B. *J. Am. Chem. Soc.* **1966**, *88*, 2874−2876.

(5) Sproules, S.; Weyhermüller, T.; DeBeer, S.; Wieghardt, K. *Inorg. Chem.* **2010**, *49*, 5241−5261.

(6) Livage, C.; Fourmigué, M.; Batail, P.; Canadell, E.; Coulon, C. *Bull. Soc. Chim. Fr.* **1993**, *130*, 761−771.

(7) Smith, A. E.; Schrauzer, G. N.; Mayweg, V. P.; Heinrich, W. *J. Am. Chem. Soc.* **1965**, *87*, 5798−5799.

(8) Lim, B. S.; Donahue, J. P.; Holm, R. H. *Inorg. Chem.* **2000**, *39*, 263−273.

(9) Friedle, S.; Partyka, D. V.; Bennett, M. V.; Holm, R. H. *Inorg. Chim. Acta* **2006**, *359*, 1427−1434.

(10) Wang, K.; McConnachie, J. M.; Stiefel, E. I. *Inorg. Chem.* **1999**, *38*, 4334−4341.

(11) Chandrasekaran, P.; Arumugam, K.; Jayarathne, U.; Pérez, L. M.; Mague, J. T.; Donahue, J. P. *Inorg. Chem.* **2009**, *48*, 2103−2113.

(12) Goddard, C. A.; Holm, R. H. *Inorg. Chem.* **1999**, *38*, 5389−5398.

(13) (a) Eisenberg, R.; Brennessel, W. W. *Acta Crystallogr.* **2006**, *C62*, m464−m466. (b) Eisenberg, R.; Ibers, J. A. *J. Am. Chem. Soc.* **1965**, *87*, 3776−3778. (c) Eisenberg, R.; Ibers, J. A. *Inorg. Chem.* **1966**, *5*, 411−416.

(14) Sproules, S.; Benedito, F. L.; Bill, E.; Weyhermüller, T.; DeBeer George, S.; Wieghardt, K. *Inorg. Chem.* **2009**, *48*, 10926−10941.

(15) Tenderholt, A. L.; Szilagyi, R. K.; Holm, R. H.; Hodgson, K. O.; Hedman, B.; Solomon, E. I. *Inorg. Chem.* **2008**, *47*, 6382−6392.

(16) Bailar, J. C. *J. Inorg. Nucl. Chem.* **1958**, 165−175.

(17) Schrauzer, G. N.; Mayweg, V. P.; Heinrich, W. *J. Am. Chem. Soc.* **1966**, *88*, 5174−5179.

(18) (a) Schrauzer, G. N. *Acc. Chem. Res.* **1969**, *2*, 72−80. (b) Schrauzer, G. N. *Trans. Met. Chem.* **1968**, *4*, 299−335.

(19) Darensbourg, D. J.; Draper, J. D.; Frost, B.; Reibenspies, J. H. *Inorg. Chem.* **1999**, *38*, 4705−4714.

(20) Nemykin, V. N.; Olsen, J. G.; Perera, E.; Basu, P. *Inorg. Chem.* **2006**, *45*, 3557−3568.

(21) Isaksson, R.; Liljefors, T.; Sandström, J. *J. Chem. Res (S)* **1981**, 43.

(22) Darensbourg, D. J.; Kump, R. L. *Inorg. Chem.* **1978**, *17*, 2680−2682.

(23) Armarego, W. L.; Perrin, D. D. *Purification of Laboratory Chemicals*; Butterworth-Heinemann: Oxford, U.K., 2000.

(24) Hanson, G. R.; Gates, K. E.; Noble, C. J.; Griffin, M.; Mitchell, A.; Benson, S. *J. Inorg. Biochem.* **2004**, *98*, 903−916.

(25) Frisch, M. J.; Trucks, G. W.; Schlegel, H. B.; Scuseria, G. E.; Robb, M. A.; Cheeseman, J. R.; Scalmani, G.; Barone, V.; Mennucci, B.; Peterson, G. A.; Nakatsuji, H.; Caricato, M.; Li, X.; Hratchian, H. P.; Izmaylov, A. F.; Bloino, J.; Zheng, G.; Sonnenberg, J. L.; Hada, M.; Ehara, M.; Toyota, K.; Fukuda, R.; Hasegawa, J.; Ishida, M.; Nakajima, T.; Honda, Y.; Kitao, O.; Nakai, H.; Vreven, T.; Montgomery, Jr., J. A.;

Peralta, J. E.; Ogliaro, F.; Bearpark, M.; Heyd, J. J.; Brothers, E.; Kudin, K. N.; Staroverov, V. N.; Kobayashi, R.; Normand, J.; Raghavachari, K.; Rendell, A.; Burant, J. C.; Iyengar, S. S.; Tomasi, J.; Cossi, M.; Rega, N.; Millam, N. J.; Klene, M.; Knox, J. E.; Cross, J. B.; Bakken, V.; Adamo, C.; Jaramillo, J.; Gomperts, R.; Stratmann, R. E.; Yazyev, O.; Austin, A. J.; Cammi, R.; Pomelli, C.; Ochterski, J. W.; Martin, R. L.; Morokuma, K.; Zakrzewski, V. G.; Voth, G. A.; Salvador, P.; Dannenberg, J. J.; Dapprich, S.; Daniels, A. D.; Farkas, Ö.; Foresman, J. B.; Ortiz, J. V.; Cioslowski, J.; Fox, D. J. *Gaussian 09*, Revision A.1; Gaussian Inc.: Wallingford, CT, 2009.

(26) (a) Becke, A. D. *J. Chem. Phys.* **1993**, *98*, 5648−5652. (b) Lee, C. T.; Yang, W. T.; Parr, R. G. *Phys. Rev. B* **1988**, *37*, 785−789.

(27) http://bse.pnl.gov/bse/portal.

(28) (a) Dunning, Jr., T. H. Jr. *J. Chem. Phys.* **1971**, *55*, 716−723. (b) Klatt, G.; Willets, A.; Handy, N. C. *Chem. Phys. Lett.* **1996**, *249*, 272−278.

(29) *Jmol*, an open-source Java viewer for chemical structures in 3D; http://jmol.sourceforge.net/.

(30) *Chemcraft*, Version 1.6; http://www.chemcraftprog.com.

(31) Tenderholt, A. L. *QMForge: A Program to Analyze Quantum Chemistry Calculations*, Version 2.1; http://qmforge.sourceforge.net.

(32) Neese, F. *Orca, an Ab Initio, Density Functional and Semiempirical Electronic Structure Program Package*, version 2.8; Universität Bonn: Bonn, Germany, 2010.

(33) (a) Weigend, F.; Ahlrichs, R. *Phys. Chem. Chem. Phys.* **2005**, *7*, 3297−3305. (b) Pantazis, D. A.; Chen, X.-Y.; Landis, C. R.; Neese, F. *J. Chem. Theory Comput.* **2008**, *4*, 908−919.

(34) (a) van Lenthe, E.; Baerends, E. J.; Snijders, J. G. *J. Chem. Phys.* **1993**, *99*, 4597−4610. (b) van Lenthe, E.; Baerends, E. J.; Snijders, J. G. *J. Chem. Phys.* **1994**, *101*, 9783−9792. (c) van Wüllen, C. *J. Chem. Phys.* **1998**, *109*, 392−399.

(35) Klamt, A.; Schüürmann, G. *J. Chem. Soc., Perkin Trans. 2* **1993**, 799−805.

(36) *Molekel*, Advanced Interactive 3D-Graphics for Molecular Sciences; Swiss National Supercomputing Center; http://www.cscs.ch/molekel.

(37) (a) Becke, A. D. *J. Chem. Phys.* **1986**, *84*, 4524−4529. (b) Perdew, J. P. *Phys. Rev. B* **1986**, *33*, 8822−8824.

(38) (a) DeBeer George, S.; Petrenko, T.; Neese, F. *Inorg. Chim. Acta* **2008**, *361*, 965. (b) Ray, K.; DeBeer George, S.; Solomon, E. I.; Wieghardt, K.; Neese, F. *Chem.—Eur. J.* **2007**, *13*, 2783.

(39) (a) Bosman, W. P.; Nieuwpoort, A. *Inorg. Chem.* **1976**, *15*, 775−780. (b) Enemark, J. H.; Cooney, J. J. A.; Wang, J.-J.; Holm, R. H. *Chem. Rev.* **2004**, *104*, 1175−1200, , and references cited therein. (c) Groysman, S.; Holm, R. H. *Inorg. Chem.* **2007**, *46*, 4090−4102. (d) Jiang, J.; Holm, R. H. *Inorg. Chem.* **2004**, *43*, 1302−1310. (e) Majumdar, A.; Pal, K.; Sarkar, S. *Inorg. Chem.* **2008**, *47*, 3393−3401. (f) Majumdar, A.; Sarkar, S. *Inorg. Chim. Acta* **2009**, *362*, 3493−3501. (g) Wang, J.-J.; Tessier, C.; Holm, R. H. *Inorg. Chem.* **2006**, *45*, 2979−2988.

(40) Lang, R. F.; Ju, T. D.; Bryan, J. C.; Kubas, G. J.; Hoff, C. D. *Inorg. Chim. Acta* **2003**, *348*, 157−164.

(41) Nicholas, K. M.; Khan, M. A. *Inorg. Chem.* **1987**, *26*, 1633−1636.

(42) Miao, M.; Willer, M. W.; Holm, R. H. *Inorg. Chem.* **2000**, *39*, 2843−2849.

(43) (a) Baker, P. K.; Drew, M. G. B.; Parker, E. E.; Robertson, N.; Underhill, A. E. *J. Chem. Soc., Dalton Trans.* **1997**, 1429−1433. (b) Barnard, K. R.; Wedd, A. G.; Tiekink, E. R. T. *Inorg. Chem.* **1990**, *29*, 891−892.

(44) (a) Cleland, W. E. Jr.; Barnhart, K. M.; Yamanouchi, K.; Collison, D.; Mabbs, F. E.; Ortega, R. B.; Enemark, J. H. *Inorg. Chem.* **1987**, *26*, 1017−1025. (b) Dhawan, I. K.; Enemark, J. H. *Inorg. Chem.* **1996**, *35*, 4873−4882. (c) Dhawan, I. K.; Pacheco, A.; Enemark, J. H. *J. Am. Chem. Soc.* **1994**, *116*, 7911−7912. (d) Drew, S. C.; Hill, J. P.; Lane, I.; Hanson, G. R.; Gable, R. W.; Young, C. G. *Inorg. Chem.* **2007**, *46*, 2373−2387. (e) Eagle, A. A.; Harben, S. M.; Tiekink, E. R. T.; Young, C. G. *J. Am. Chem. Soc.* **1994**, *116*, 9749−9750. (f) Inscore, F. E.; Joshi, H. K.; McElhaney, A. E.; Enemark, J. H. *Inorg. Chim. Acta*

2002, *331*, 246−256. (g) Inscore, F. E.; Knottenbelt, S. Z.; Rubie, N. D.; Joshi, H. K.; Kirk, M. L.; Enemark, J. H. *Inorg. Chem.* **2006**, *45*, 967−976. (h) Lim, P. J.; Slizys, D. A.; Tiekink, E. R. T.; Young, C. G. *Inorg. Chem.* **2005**, *44*, 114−121. (i) Sproules, S. A.; Morgan, H. T.; Doonan, C. J.; White, J. M.; Young, C. G. *Dalton Trans.* **2005**, 3552−3557. (j) Young, C. G.; Gable, R. W.; Hill, J. P.; George, G. N. *Eur. J. Inorg. Chem.* **2001**, 2227−2231.

(45) De Ridder, D. J. A. *Acta Crystallogr., Sect. C* **1993**, *49*, 1975−1976.

(46) (a) Lim, B. S.; Fomitchev, D. V.; Holm, R. H. *Inorg. Chem.* **2001**, *40*, 4257−4262. (b) Bigoli, F.; Chen, C.-T.; Wu, W.-C.; Deplano, P.; Mercuri, M. L.; Pellinghelli, M. A.; Pilia, L.; Pintus, G.; Serpe, A.; Trogu, E. F. *Chem. Commun.* **2001**, 2246−2247.

(47) Sproules, S.; Banerjee, P.; Weyhermüller, T.; Yan, Y.; Donahue, J. P.; Wieghardt, K. *Inorg. Chem.* **2011**, *50*, 7106−7122.

(48) Albright, T. A.; Burdett, J. K.; Whangbo, M.-H. *Orbital Interactions in Chemistry, 1*; John Wiley and Sons, Inc.: New York, 1985.

(49) The actual HOMO will vary because of small geometrical changes depending on the calculation parameters used.

(50) (a) Raymond, K. N.; Isied, S. S.; Brown, L. D.; Fronczek, F. R.; Nibert, J. H. *J. Am. Chem. Soc.* **1976**, *98*, 1767−1774. (b) Wunderlich, H.; Mootz, D. *Acta Crystallogr., Sect. B* **1971**, *27*, 1684−1686.

(51) Kapre, R. R.; Bothe, E.; Weyhermüller, T.; DeBeer George, S.; Muresan, N.; Wieghardt, K. *Inorg. Chem.* **2007**, *46*, 7827−7839.

(52) Ye, Q.; Wu, Q.; Zhao, H.; Song, Y.-M.; Xue, X.; Xiong, R.-G.; Pang, S.-M.; Lee, G.-H. *J. Organomet. Chem.* **2005**, *690*, 286−290.

(53) (a) Miholová, D.; Gaš, B.; Záliš, S.; Klíma, J.; Vlček, A. A. *J. Organomet. Chem.* **1987**, *330*, 75−84. (b) Scarborough, C. C.; Weighardt, K. *Inorg. Chem.* **2011**, *50*, 9773−9793.

(54) See Supporting Information for a complete listing of the results of the survey of the Cambridge Structural Database organized by geometry of the $W(CO)_4$ fragment.

(55) (a) Barr, M. E.; Smith, S. K.; Spencer, B.; Dahl, L. F. *Organometallics* **1991**, *10*, 3983−3991. (b) Cotton, F. A.; Falvello, L. R.; Meadows, J. H. *Inorg. Chem.* **1985**, *24*, 514−517. (c) Drew, M. G. B.; Wilkins, J. D. *J. Organomet. Chem.* **1974**, *69*, 271−278. (d) Faggiani, R.; Gillespie, R. J.; Campana, C.; Kolis, J. W. *J. Chem. Soc., Chem. Commun.* **1987**, 485−486. (e) Górski, M.; Kochel, A.; Szymańska-Buzar, T. *J. Organomet. Chem.* **2006**, *691*, 3708−3714. (f) Hart, I. J.; Jeffrey, J. C.; Grosse-Ophoff, M. J.; Stone, F. G. A. *J. Chem. Soc., Dalton Trans.* **1988**, 1867−1877. (g) Jones, C.; Schulten, C.; Stasch, A. *Dalton Trans.* **2006**, 3733−3735. (h) Kramkowski, P.; Scheer, M. *Eur. J. Inorg. Chem.* **2000**, 1869−1876. (i) Levisalles, J.; Rose-Munch, F.; Rudler, H.; Daran, J.-C.; Jeannin, Y. *J. Chem. Soc., Chem. Commun.* **1981**, 1057−1058. (j) Mathur, P.; Chakrabarty, D.; Hossain, M. M.; Rashid, R. S.; Rugmini, V.; Rheingold, A. L. *Inorg. Chem.* **1992**, *31*, 1106−1108. (k) Mathur, P.; Sekar, P.; Satyanarayana, C. V. V; Mahon, M. F. *J. Chem. Soc., Dalton Trans.* **1996**, 2173−2176. (l) Mathur, P.; Trivedi, R.; Sekar, P.; Chakrabarty, D.; Hossain, M. M.; Puranik, V. G. *J. Cluster Sci.* **1996**, *7*, 191−198. (m) Scheer, M.; Herrmann, E.; Sieler, J.; Oehme, M. *Angew. Chem., Int. Ed. Engl.* **1991**, *30*, 969−971. (n) Scheer, M.; Vogel, U.; Becker, U.; Balazs, G.; Scheer, P.; Hönle, W.; Becker, M.; Jansen, M. *Eur. J. Inorg. Chem.* **2005**, 135−141. (o) Scherer, O. J.; Vondung, C.; Wolmershäuser, G. *Angew. Chem., Int. Ed. Engl.* **1997**, *36*, 1303−1305. (p) Szymańska-Buzar, T.; Głowiak, T. *J. Organomet. Chem.* **1995**, *489*, 207−214.

(56) Curtis, M. A.; Houser, E. J.; Sabat, M.; Grimes, R. N. *Inorg. Chem.* **1998**, *37*, 102−111.

(57) Bröchler, R.; Sham, I. H. T.; Bodenbinder, M.; Schmitz, V.; Rettig, S. J.; Trotter, J.; Willner, H.; Aubke, F. *Inorg. Chem.* **2000**, *39*, 2172−2177.

(58) Manuta, D. M.; Lees, A. J. *Inorg. Chem.* **1986**, *25*, 3212−3218.

(59) Stufkens, D. J. *Coord. Chem. Rev.* **1990**, *104*, 39−112.

(60) Kirin, V.; Roesky, P. W. *Z. Anorg. Allg. Chem.* **2004**, *630*, 466−469.

(61) Youssef, A. O.; Khalil, M. M. H.; Ramadan, R. M.; Soliman, A. A. *Trans. Met. Chem.* **2003**, *28*, 331−335.

(62) (a) Balk, R. W.; Stufkens, D. J.; Oskam, A. *Inorg. Chim. Acta* **1979**, *34*, 267−274. (b) Brunner, H.; Herrmann, W. A. *Chem. Ber.* **1972**, *105*, 770−783. (c) Buffin, B. P.; Squattrito, P. J.; Ojewole, A. O. *Inorg. Chem. Commun.* **2004**, *7*, 14−17. (d) Drolet, D. P.; Chan, L.; Lees, A. J. *Organometallics* **1988**, *7*, 2502−2506. (e) Heinze, K. *Chem.—Eur. J.* **2001**, *7*, 2922−2932. (f) Herrick, R. S.; Dupont, J.; Wrona, I.; Pilloni, J.; Beaver, M.; Benotti, M.; Powers, F.; Ziegler, C. J. *J. Organomet. Chem.* **2007**, *692*, 1226−1233.

(63) Stiddard, M. H. B. *J. Chem. Soc.* **1962**, 4712−4715.

(64) Farrell, I. R.; Hartl, F.; Záliš, S.; Mahabiersing, T.; Vlček, Jr., A. *J. Chem. Soc., Dalton Trans.* **2000**, 4323−4331.

(65) (a) Iravani, E.; Neumüller, B. *Z. Anorg. Allg. Chem.* **2003**, *629*, 2509−2515. (b) Yih, K.-H.; Lee, G.-H.; Huang, S.-L.; Wang, Y. *J. Organomet. Chem.* **2003**, *665*, 114−121.

(66) Glaser, T.; Hedman, B.; Hodgson, K. O.; Solomon, E. I. *Acc. Chem. Res.* **2000**, *33*, 859−868.

(67) Szilagyi, R. K.; Lim, B. S.; Glaser, T.; Holm, R. H.; Hedman, B.; Hodgson, K. O.; Solomon, E. I. *J. Am. Chem. Soc.* **2003**, *125*, 9158−9169.

(68) Geary, E. A. M.; Yellowlees, L. J.; Parsons, S.; Pilia, L.; Serpe, A.; Mercuri, M. L.; Deplano, P.; Clark, S. J.; Robertson, N. *Dalton Trans.* **2007**, 5453−5459.

(69) Carrington, A.; MacLachlan, A. D. *Introduction to Magnetic Resonance*; Harper & Row: New York, 1967.

(70) Min, K. S.; DiPasquale, A. G.; Rheingold, A. L.; White, H. S.; Miller, J. S. *J. Am. Chem. Soc.* **2009**, *131*, 6229−6236.

(71) Cremades, E.; Echeverría, J.; Alvarez, S. *Chem.—Eur. J.* **2010**, *16*, 10380−10396.

(72) Vaid, T. P.; Veige, A. S.; Lobkovsky, E. B.; Glassey, W. V.; Wolczanski, P. T.; Liable-Sands, L. M.; Rheingold, A. L.; Cundari, T. R. *J. Am. Chem. Soc.* **1998**, *120*, 10067−10079.

(73) Raehm, L.; Sauvage, J.-P. *Struct. Bonding (Berlin)* **2001**, *99*, 55−78.

(74) Hawthorne, M. F.; Ramachandran, B. M.; Kennedy, R. D.; Knobler, C. B. *Pure Appl. Chem.* **2006**, *78*, 1299−1304.